

CERN-EP-2021-146
21 July 2021

K_S^0 - and (anti-) Λ -hadron correlations in pp collisions at $\sqrt{s} = 13$ TeV

ALICE Collaboration*

Abstract

Two-particle azimuthal correlations are measured with the ALICE apparatus in pp collisions at $\sqrt{s} = 13$ TeV to explore strangeness- and multiplicity-related effects in the fragmentation of jets and the transition regime between bulk and hard production, probed with the condition that a strange meson (K_S^0) or a baryon (Λ) with transverse momentum $p_T > 3$ GeV/c is produced. Azimuthal correlations between kaons or Λ hyperons with other hadrons are presented at midrapidity for a broad range of the trigger ($3 < p_T^{\text{trigg}} < 20$ GeV/c) and associated particle p_T (1 GeV/c $< p_T^{\text{assoc}} < p_T^{\text{trigg}}$), for minimum-bias events and as a function of the event multiplicity. The near- and away-side peak yields are compared for the case of either K_S^0 or $\Lambda(\bar{\Lambda})$ being the trigger particle with that of inclusive hadrons (a sample dominated by pions). In addition, the measurements are compared with predictions from PYTHIA 8 and EPOS LHC event generators.

arXiv:2107.11209v1 [nucl-ex] 23 Jul 2021

1 Introduction

Particle production as a function of the event charged-particle multiplicity in proton-proton (pp) collisions at the LHC has revealed interesting patterns. Clearly, in the soft (bulk) particle production domain with low transverse momentum ($p_T \lesssim 4$ GeV/c), several experimental measurements indicate features in high-multiplicity pp collisions similar to those observed in nucleus–nucleus collisions. These include long-range correlations in pseudorapidity [1, 2], large azimuthal anisotropies [3, 4] and strangeness production [5, 6].

These measurements are theoretically interpreted in terms of a combination of initial-state collective dynamics (colour-glass condensate) [7] or as a hydrodynamic-like (final-state) collective flow [8]. Quantifying the relative contributions of initial- and final-state phenomena is a challenge, both experimentally and theoretically (see reviews [9, 10]). These phenomena are also modelled in Monte Carlo (MC) event generators, like PYTHIA8 [11] or EPOS LHC [12]. For example, a basic experimental finding in pp collisions, the increase of the average transverse momentum with the event multiplicity is realized in these two models very differently. In PYTHIA 8, in events with several partonic scatterings, termed Multiple Parton Interactions (MPI), the respective color strings cut (reconnect) each other, leading to a redistribution of energy from particle production to transverse momentum. In the EPOS LHC model, a parametrised hydrodynamic evolution of a small volume with high density of thermalised matter (core) is used. In both models the respective parameters were tuned using the Run 1 data at the LHC, without explicit inclusion of particle correlations [12, 13].

In PYTHIA8, correlations among the final state hadrons are realized through transversely extended strings, exerting on each other transverse shoves [14] that mimic collective dynamics, akin to that of a (long-lived) quark–gluon medium. The shoving model of hadronisation was recently used to discern within a PYTHIA8 study [15] possible effects of jet quenching in pp collisions. This prominent characteristic of nucleus–nucleus collisions, remains undetected in high-multiplicity pp or p–Pb collisions [16], perhaps not surprisingly, given the much smaller spatial extension of the dense system, compared to the nucleus–nucleus case. Experimentally, it was recently shown that in pp collisions the near-side long-range (in pseudorapidity) ridge yield (of bulk particles) in high-multiplicity events remains present for events which are additionally biased, through either a Z boson [17], a leading high- p_T particle or a jet [18]. These findings are interesting per se and also motivate the quest to find or exclude jet quenching in high-multiplicity events in small collision systems, with differences in the observed effects on gluon, light and heavy quark jets.

At LEP, differences between quark- and gluon-initiated jets in e^+e^- annihilations have been revealed in several measurements. Gluon jets are characterised by a larger charged-particle multiplicity than quark jets [19, 20]. Moreover, in the relative production of K_S⁰ mesons and Λ hyperons to charged particles, it was found that the relative production of Λ is $\approx 30\%$ higher in gluon than in quark jets, while the relative K_S⁰ production was found to be approximately the same [21].

In the present article, such studies of particle production and correlations are continued, exploring the effect of a strangeness bias, both in form of a meson (K_S⁰) or a baryon (Λ) with $p_T > 3$ GeV/c. The correlations between kaons or Λ($\bar{\Lambda}$) hyperons with other hadrons are studied at midrapidity in pp collisions at $\sqrt{s} = 13$ TeV for a broad range of the trigger ($3 < p_T^{\text{trigg}} < 20$ GeV/c) and associated particle p_T (1 GeV/c $< p_T^{\text{assoc}} < p_T^{\text{trigg}}$), for minimum bias events and as a function of the event multiplicity measured at forward rapidities. Such correlations encode effects of fragmentation, hadronisation and parton showering as well as possible collectivity and jet quenching. The complex overlap of these aspects is probed through the experimental handles of particle species and p_T , inducing different kinematic and flavour biases. The near- and away-side peak yields are compared for the case of either K_S⁰ or (anti-)Λ as a trigger particle with that of inclusive hadrons (a sample dominated by pions). The measurements are, in addition, compared with the PYTHIA 8 and EPOS LHC event generators.

The article is organised as follows: Section 2 outlines the experimental setup and the data sample; Section 3 describes the analysis, while Section 4 presents the results; a summary and an outlook are given in Section 5.

2 Experiment and data sample

The inclusive charged hadron, K_S^0 meson and (anti-) Λ hyperon identification at midrapidity is performed using the tracking detectors of the ALICE central barrel located in a solenoidal magnet, which provides a magnetic field of 0.5 T oriented along the beam direction. A detailed description of the ALICE experiment and its performance can be found in [22, 23].

2.1 Event selection

For the data taking, a minimum bias (MB) trigger is employed, provided by the V0 detector, which consists of two forward scintillator arrays covering the pseudorapidity ranges $-3.7 < \eta < -1.7$ and $2.8 < \eta < 5.1$. The MB trigger signal consists of a coincident signal in both arrays. All events selected in this analysis are required to have a reconstructed primary collision vertex (PV) within the longitudinal interval $|z_{\text{vtx}}| < 10$ cm from the nominal interaction point in order to ensure uniform detector performance. Beam-gas events are rejected using timing cuts with the V0 detector. Moreover pile-up events are rejected based on the Silicon Pixel Detector (SPD) information. The total number of analysed pp collisions at $\sqrt{s} = 13$ TeV, measured during the LHC Run 2 data-taking period in years 2016–2018 by ALICE is 1.58×10^9 corresponding to integrated luminosity of about 27 nb^{-1} .

2.2 Multiplicity selection

The correlation functions are calculated for six event classes (0–1%, 1–3%, 3–7%, 7–15%, 15–50%, 50–100%), selected on the event activity via the multiplicity in the forward and backward direction, measured with the V0 detector within the acceptance described above. The events are selected based on percentiles of the summed signal in the two V0 detectors (V0M), for instance the 0–1% and 50–100% classes are the events with the highest and lowest range of the V0M signal. The trigger efficiency is not accounted for in the above multiplicity ranges. The intervals corrected for the trigger efficiency are: respectively; 0–0.92%, 0.92–2.74%, 2.74–6.40%, 6.40–13.44%, 13.44–46.12%, 46.12–100% [24].

For the MC event generators, the multiplicity classes are selected with the trigger-corrected percentile calculation, applied to the distribution of charged primary particles produced in the η acceptance of the V0 detectors.

2.3 Primary hadron and V^0 selection

Primary charged tracks (denoted as h) are reconstructed in the pseudorapidity range $|\eta| < 0.8$ using the Inner Tracking System (ITS), which consists of six layers of silicon detectors around the beam pipe, and the Time Projection Chamber (TPC), consisting of a large cylindrical drift volume filled with nearly 90 m^3 either of Ar/CO₂ (88/12, in 2016 and 2018) or Ne/CO₂/N₂ (90/10/5 in 2017) and read out by multi-wire proportional chambers. Combining the information from these two detectors, the primary charged-track sample is created by applying selection criteria in order to suppress the contamination from secondary particles following previous studies [25]. The number of crossed pad rows in the TPC is required to be at least 70 (out of a maximum of 159) and the minimal ratio to the number of findable clusters (geometrically possible assignable clusters to a track) is 0.8. Only tracks with a fraction of shared clusters with other tracks smaller than 0.4 are accepted. The distance of closest approach (DCA) to the PV is required to be within an ellipsoid with semi-axes of 2.4 cm and 3.2 cm in the xy -plane and z -direction, respectively. Every track is required to have a fit quality for both TPC and ITS, characterised by goodness-of-fit values χ^2 per cluster smaller than 4 and 36 for the TPC and ITS, respectively. Only

tracks with a hit in the two most inner layers of ITS are selected. The kink topologies produced by decays are rejected. The selected sample of primary charged particles is dominated by hadrons. The electrons constitute less than 1%.

Table 1: Selection criteria for V^0 candidates based on the topological variables.

Selection criterion	K_S^0	$\Lambda(\bar{\Lambda})$
Absolute value of rapidity	< 0.5	< 0.5
Decay radius (cm)	> 0.5	> 0.5
DCA _{xy} of daughter track to PV (cm)	> 0.06	> 0.06
DCA _{xy} between daughter tracks ($n\sigma$)	< 1	< 1
$\cos(\theta_{PA})$	> 0.97	> 0.995
Proper lifetime (cm)	< 20	< 30
Competing rejection (GeV/c^2)	> 0.005	> 0.01
Invariant mass (GeV/c^2)	$m_{K_S^0} \pm 3\sigma$	$m_{\Lambda(\bar{\Lambda})} \pm 3\sigma$

The K_S^0 mesons and $\Lambda(\bar{\Lambda})$ baryons (V^0 particles) are reconstructed in the rapidity range $|y| < 0.5$ via their most probable decay channels [26] and exploiting their characteristic (V^0) decay topology:

$$\begin{aligned} K_S^0 &\rightarrow \pi^+ + \pi^- (69.2\%), \\ \Lambda &\rightarrow p + \pi^- (63.9\%), \\ \bar{\Lambda} &\rightarrow \bar{p} + \pi^+ (63.9\%). \end{aligned}$$

The identification and reconstruction follows previous measurements presented in [27] and [28]. The identification of the daughter tracks is performed via specific energy loss dE/dx in the TPC, which is required to be within $\pm 3\sigma$ from the expected mean value for pions or protons (for more details see [23]). The track quality criteria are the same as for the primary global tracks described above. The pairs of identified daughter tracks are combined to V^0 candidates, which are accepted if their invariant mass is within 3σ (1σ for K_S^0 is in the range 0.0039-0.0075 GeV/c^2 and for Λ in 0.0021-0.0033 GeV/c^2 depending on p_T) from the nominal value. The combinatorial contribution is suppressed by applying selection criteria based on the topological variables summarised in Table 1. Here, the V^0 decay radius is the distance between the point where the V^0 decays (secondary vertex) and the PV. The DCA_{xy} to PV is the distance of closest approach between the daughter track and the PV. The θ_{PA} refers to the pointing angle, which is the angle between the momentum vector of the V^0 candidate and the line connecting the primary and secondary vertex. The reconstructed proper lifetime of an individual particle is defined as mL/p , where m is the particle mass, L is the distance between primary and secondary vertex and p is the particle momentum. The mean life $c\tau$ is listed in [26] and its value is 2.68 cm and 7.89 cm for K_S^0 and $\Lambda(\bar{\Lambda})$, respectively. It can happen that a certain pair reconstructed as K_S^0 candidate can have an invariant mass of $\Lambda(\bar{\Lambda})$ under the $p\pi$ assumption for the daughter tracks. Such pairs are not accepted neither as K_S^0 nor as $\Lambda(\bar{\Lambda})$ candidates. Table 1 quotes under the competing rejection entry the mass on which this criterion is applied for both K_S^0 and Λ . Besides the topological selections, a bunch-off pile-up (by the high frequency collisions, some tracks from previous bunch-crossing remain in TPC when current collision happen) removal criterion is required where at least one of the V^0 daughter tracks is reconstructed both in ITS and TPC or has a signal in the Time-Of-Flight detector.

3 Analysis

3.1 The correlation function

In the dihadron correlation approach, the first hadron is the trigger particle, here either a primary charged particle (hadron) or an identified K_S^0 meson or $\Lambda(\bar{\Lambda})$ hyperon with p_T in range 3-20 GeV/c . Since the Λ -

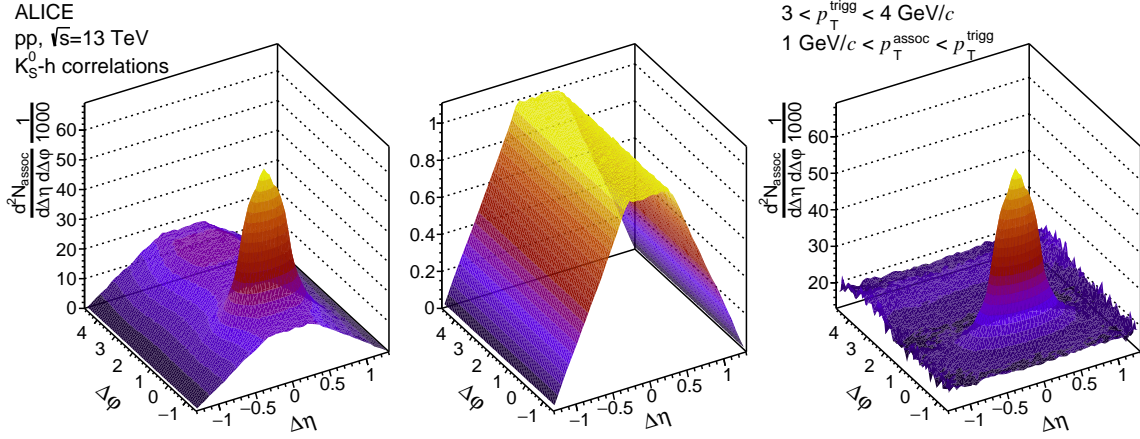


Figure 1: An example of the raw same-event (left), mixed-event (middle) and final (mixed-event scaled, right) two-dimensional correlation function for K_S^0 -hadrons. The correlation functions were scaled with $1/1000$ for better visibility. The plateau in the left and middle plot is caused by non-equal selection in η of the trigger and associated particle.

h and $\bar{\Lambda}$ - h correlation functions are compatible, as expected for this collision energy, the results are combined and reported in the following as $(\Lambda + \bar{\Lambda})$ - h . The second particle is the associated particle, in this case, always a primary charged particle with a kinematic requirement $1 \text{ GeV}/c < p_T^{\text{assoc}} < p_T^{\text{trigg}}$. By calculating the differences in the azimuthal angle and pseudorapidity for each of such pairs, three types of correlation functions are constructed: h - h , K_S^0 - h and $(\Lambda + \bar{\Lambda})$ - h . Pairs with invariant mass (IM) within $\text{IM} \pm 5 \text{ MeV}/c^2$ of a resonance (K_S^0 , Λ , γ , ρ , ϕ , Δ^+ , J/ψ , K^* , D^0 , Δ^{++}) are not accepted in the case of h - h . In the case of $(\Lambda + \bar{\Lambda})$ - h correlations, this restriction is applied to pairs with IM of a cascade (Σ , Ξ , Ω). An example of a raw K_S^0 - h correlation function is shown in Fig. 1 (left panel). At $(\Delta\phi, \Delta\eta) = (0, 0)$, one can observe the near-side peak, which originates mostly from particle pairs fragmented within the same jet. Bose-Einstein correlations, strong decays of high-mass resonances and final state interactions may have also a small contribution for the h - h case. Due to momentum conservation, jets are produced back-to-back in the transverse plane. Thus, a second peak around π in $\Delta\phi$ is expected, which is smeared in the $\Delta\eta$ direction, because the particles can obtain an additional longitudinal boost related to the varied center-of-mass frame of the partonic collision. In the selection of the trigger particle, the near-side jet is fully reconstructed in the longitudinal direction, but the away-side jet is not necessarily (fully) within the detector acceptance. The procedure of getting fully corrected 2-dimensional per-trigger yield is schematically written in Eq 1. Here, $\frac{d^2 N_{\text{pair}}^{\text{raw}}}{d\Delta\phi d\Delta\eta}(\Delta\phi, \Delta\eta)$ is the uncorrected correlation function, ϵ_{trigg} , ϵ_{assoc} and ϵ_{pair} are correction factors further described in Sec. 3.2 and N_{trigg} is the number of the trigger particles. Afterwards, the 2-dimensional per-trigger yield is projected on the $\Delta\phi$ axis and integrated (see Eq. 2) in the intervals $|\Delta\phi| < 0.9$ and $|\Delta\phi - \pi| < 1.4$ to obtain the near-side and away-side yield, respectively, denoted as $Y_{\Delta\phi}$ in Eq. 2.

$$\frac{d^2 N_{\text{pair}}}{d\Delta\phi d\Delta\eta}(\Delta\phi, \Delta\eta) = \frac{1}{N_{\text{trigg}}} \frac{1}{\epsilon_{\text{trigg}}} \frac{1}{\epsilon_{\text{assoc}}} \frac{d^2 N_{\text{pair}}^{\text{raw}}}{d\Delta\phi d\Delta\eta}(\Delta\phi, \Delta\eta) \frac{1}{\epsilon_{\text{pair}}} \quad (1)$$

$$Y_{\Delta\phi} = \int_{\Delta\phi_1}^{\Delta\phi_2} \frac{dN}{d\Delta\phi} d\Delta\phi \quad (2)$$

3.2 Corrections

The corrections are described in the same order as they were applied to the data.

All MC-based corrections are calculated using events from PYTHIA8.210 (Monash 2013 tune) [13, 29], with particle propagation through the detector by means of GEANT3 [30]. The detection inefficien-

cies are corrected with the single particle efficiency factor, calculated in MC and applied as weight ($1/\epsilon_{\text{trigg}} \times 1/\epsilon_{\text{assoc}}$) for each pair. This factor was calculated separately for trigger and associated particles as a function of p_T , η , ϕ and PV position. In the case of primary charged particles, a p_T -dependent contamination factor is also part of the weight to account for the amount of secondary particles in the sample. This is defined as a ratio of only primary tracks to all reconstructed ones.

Imperfect detector acceptance within $|\eta| < 0.8$ range is corrected with the mixed-event method, where trigger particles from one event are correlated with associated particles from different events. Thus, no physical correlations are present. The mixed-event correlation function has a typical triangular shape determined by the η acceptance. An example of this function is shown in the middle plot of Fig. 1 where a plateau is visible. This is caused by different ranges in η for trigger (K_S^0) and associated particles (h). The mixed-event correlation is already scaled to unity with a scaling factor equal to the average of bins with $\Delta\eta = 0$. In the following, the actual correlation function is divided by the mixed-event one to eliminate the detector acceptance effects as illustrated in Fig. 1. This correction is schematically written as $1/\epsilon_{\text{pair}}$ in Eq. 1. In some cases, due to the finite binning in multiplicity and PV position in z-direction, the mixed-event correlation does not match the shape of the background perfectly. For this reason, a so called ‘‘wing’’ correction is performed. Here the correlation function is scaled once more with a 2D distribution constant in $\Delta\phi$ and dependent on $\Delta\eta$ in order to get a flat distribution in $\Delta\eta$ at the away-side. This correction is never larger than 2% and only affects the h-h correlation function. A similar effect was observed also in previous analysis [31].

For the reconstruction of K_S^0 mesons and $\Lambda(\bar{\Lambda})$ baryons, some of the candidates selected with the topological criteria are in fact combinatorial background. Since the shape of the correlation function does not need to be the same for the signal and background, a second correlation function is calculated, where candidates from two intervals from outside the invariant mass peak ($m_{V^0} - 9\sigma$ to $m_{V^0} - 6\sigma$ and $m_{V^0} + 6\sigma$ to $m_{V^0} + 9\sigma$) are taken as trigger particles. These give the same width as the signal region in the invariant mass spectrum. The second ‘‘side-band’’ correlation function is subtracted from the signal one. The number of trigger particles is in addition corrected for purity, defined as a ratio of number of signal V^0 candidates over all candidates within the invariant mass acceptance region.

In the case of $\Lambda(\bar{\Lambda})$ being the trigger particle, the feed-down contribution from decays of Ξ (the Ξ are reconstructed following [6]) baryons is subtracted in a similar way as for the combinatorial background. For this case, the $(\Xi^- + \Xi^+)$ -h correlation function in every p_T and multiplicity bin is calculated, scaled with the detection efficiency of $\Lambda(\bar{\Lambda})$ from Ξ decays and subtracted from the $(\Lambda + \bar{\Lambda})$ -h correlation function. Similarly, the feed-down fraction is subtracted from the number of trigger particles. It is assumed that the production rates of charged and neutral Ξ baryons are equal and the feed-down fraction from Ω is negligible. This correction has an effect of 5% on the finale near-side yields for low p_T and smaller than 1% for high p_T .

After projecting the per-trigger yield on the $\Delta\phi$ axis, the underlying event background is subtracted with the ZYAM (Zero Yield At Minimum) method [32]. The background is assumed to be flat and estimated as the average value of six bins outside the jet peaks to reduce the statistical fluctuations.

3.3 Systematic uncertainties

The sources of systematic uncertainties of the per-trigger yields in the minimum bias sample are listed in Tab. 2. These are estimated by varying track-selection criteria and other parameters in the analysis. The significance of each source of systematic uncertainty was checked according to the Barlow criterion [33]. Within this procedure a threshold value (1σ) is set, based on which each variation can be checked, whether it is within statistical fluctuations or a real systematic difference. If a certain variation did not pass the test, this contribution was not accounted for in the total systematic uncertainty, which was calculated as a quadrature sum of the individual contributions. For the ratios of yields, the systematic uncertainties are calculated separately which causes cancellation of correlated uncertainties.

Table 2: Summary of the main sources and values of the relative systematic uncertainties (expressed in %) for the per-trigger yields in the MB sample. The abbreviation “negl.” stands for negligible (smaller than 0.1%) and “rej.” means that this variation was rejected due to the Barlow criterion.

	h-h		K_S^0 -h		$\Lambda(\bar{\Lambda})$ -h	
	near	away	near	away	near	away
$\Delta\phi$ window	0.3	0.4	0.5	0.7	0.7	0.5
PV along the z-axis (z_{vtx})	negl.	negl.	1.2	1.7	0.6	0.7
Binning in z_{vtx}	negl.	0.4	0.8	1.6	0.5	1.2
Yield calculation	1.0	negl.	1.1	0.7	0.3	0.4
Pedestal subtraction	0.8	1.9	0.4	1.6	1.0	2.0
$\Delta\eta$ range	0.5	–	1.2	–	1.0	–
Mixing scale	negl.	negl.	0.7	0.9	0.3	0.5
Topological variables	–	–	1.5	3.5	3.0	3.1
Invariant mass range	–	–	rej.	rej.	1.2	1.8
Primary track selection	0.3	0.7	1.1	1.8	2.2	0.4
Wing correction	1.2	1.8	–	–	0.7	0.8
Ξ topological variables	–	–	–	–	0.4	1.6
MC closure	negl.	negl.	negl.	negl.	2.5	negl.
Total	1.9	2.7	3.1	5.1	5.1	4.8

For the uncertainty related to the $\Delta\phi$ integration window, the window is varied around the nominal values ($|\Delta\phi| < 0.9$ and $|\Delta\phi - \pi| < 1.4$) within ± 0.1 . For the yields for the h-h correlations, on both near- and away-side, the contribution to the total uncertainty is around 0.4% for all multiplicity classes. For the yields for K_S^0 -h and $(\Lambda + \bar{\Lambda})$ -h correlations, the value varies within 0.4–2% for both near- and away-side.

The PV selection along the z-axis (z_{vtx}) is decreased from ± 10 cm to ± 7 cm from the interaction point in order to estimate the uncertainty connected to the detector acceptance effects. The uncertainty is smaller than 0.3% in all multiplicity classes for the yields from h-h correlation function. It is in the range 0.7–2.3% and 0.7–2.7% for the near-side yield in case of K_S^0 -h and $(\Lambda + \bar{\Lambda})$ -h yields, respectively. For the away-side, this source contributes with 1.7–4.5% and 0.7–4.9% in case of K_S^0 -h and $(\Lambda + \bar{\Lambda})$ -h yields, respectively.

The number of bins in z_{vtx} used for the event-mixing classes is changed from 9 to 7 to account for the uncertainty connected with the detector acceptance. For the yields triggered with an unidentified hadron, the contribution from this source is smaller than 0.5% at both sides for all multiplicity classes. This uncertainty is in the range 0.5–2.7% and 0.4–1.5% for the near-side yield triggered with K_S^0 and $(\Lambda + \bar{\Lambda})$, respectively and within 1.2–5.2% and 0.8–2.8% for the away-side.

The contribution to the systematic uncertainty resulting from the yield calculation method is estimated by fitting each jet peak with a double-gaussian function and integrating the fit function to calculate the per-trigger yield instead of calculating the yield directly by the bin counting method as default. This leads to an uncertainty around 1% for the near-side and to a value smaller than 0.2% for the away-side for the h-h yields in all multiplicity classes. For most multiplicity classes this source was rejected by the Barlow criterion for the K_S^0 trigger. The non-rejected contribution is 1.1% and 0.7% for the near- and away-side, respectively. The accounted contribution to the uncertainty of yields triggered with $(\Lambda + \bar{\Lambda})$ is in the range 0.3–0.8% and 0.2–3.4% for the near-side and away-side yields, respectively.

For the variation of the underlying event subtraction method, which takes the average value of 6 bins from the left and right side of the near-side peak, a constant fit in ranges $[-\pi/2, -1]$ and $[1, \pi/2]$ is used, leading to an estimated uncertainty around 0.6% (1.5%), 2% (2.2%) and 1.8% (4.5%) for the near-

(away-) side yield from the unidentified hadron-, K_S^0 -, and $(\Lambda + \bar{\Lambda})$ -triggered correlation functions, respectively.

The $\Delta\eta$ range is varied within 0.1 around its nominal value $|\Delta\eta| < 1$ in order to estimate the uncertainty related to the near-side jet acceptance. This is estimated to be within 0.3–0.9%, 0.6–1.9%, 0.4–2.4% for h-h, K_S^0 -h and $(\Lambda + \bar{\Lambda})$ -h yields in all multiplicity classes, respectively.

The scale factor for the mixed-event correlation function is varied, which gives a negligible contribution to the total systematic uncertainty for h-h yields for both sides. This contribution for K_S^0 -h ($(\Lambda + \bar{\Lambda})$ -h) yields is estimated as 0.7–1.5% (0.2–0.4%) and 0.9–2% (0.2–0.5%) for the near and away-side yields, respectively, in different multiplicity classes.

In order to estimate the systematic uncertainty connected to the V^0 reconstruction, the values for the topological selection are varied around the nominal values. Its value is, for different multiplicity classes, in the range 1.5–5.8% (1.9–5.6%) and 2.2–7.5% (2–5.5%) for the K_S^0 ($\Lambda + \bar{\Lambda}$) triggered yields at the near- and away-side, respectively.

The ranges for the signal and for background in the invariant mass distributions are varied in order to estimate the uncertainty related to the subtraction of the contribution from misidentified K_S^0 or $(\Lambda + \bar{\Lambda})$. This source is rejected by the Barlow criterion for the K_S^0 -h yields and has a value in the range 0.5–3.9% and 1.1–4.3% for the $(\Lambda + \bar{\Lambda})$ -h triggered yields, for the near- and away-side, respectively.

The systematic uncertainty associated with the primary track selections is estimated by selecting tracks with slightly varied criteria. These are the same as the ones used for global tracks, but there is a tighter and p_T -dependent DCA requirement in the xy -plane, which means that tracks with a DCA in the xy -plane larger than $0.0105 + 0.0350/p_T^{1.1}$ are rejected. This uncertainty is smaller than 0.7% for both the near- and away-side yield for h-h for all multiplicity classes. The uncertainty intervals for K_S^0 ($(\Lambda + \bar{\Lambda})$) triggered yields are estimated as 0.9–2.4% (0.4–3.5%) and 1.3–3.9% (0.2–3.1%) for the near- and away-side yields, respectively.

The range used for the estimation of the wing correction scaling factor is varied in order to calculate the uncertainty related to this method. This contribution is not dependent on the event multiplicity.

The $\Xi^- (\bar{\Xi}^+)$ reconstruction uncertainty contributes to the uncertainty of yields triggered by $(\Lambda + \bar{\Lambda})$. This contribution is estimated by varying the topological selection of $\Xi^- (\bar{\Xi}^+)$ hyperons around their nominal values. This uncertainty is in the range 0.2–4% (0.2–3.9%) for the near(away)-side yields for events in all multiplicity classes.

The correction procedure is checked with a Monte Carlo closure test. Two correlation functions are calculated, the first one with generated MC particles and the second one with MC particles reconstructed after GEANT3 propagation using the full reconstruction and correction chain as for the experimental data. The ratio of these two correlation functions is expected to be unity. This is the case for the h-h and K_S^0 -h correlation functions, but there is a residual departure from unity for $(\Lambda + \bar{\Lambda})$ -h correlation function at the near-side of up to 2.5%, which is accounted as a systematic uncertainty.

4 Results and discussion

The $\Delta\phi$ projections of the correlation functions for the three different trigger particles are shown for two p_T^{trigg} intervals, $3 < p_T^{\text{trigg}} < 4$ GeV/ c and $9 < p_T^{\text{trigg}} < 11$ GeV/ c , in Fig. 2. Included are also the correlation functions predicted by MC event generators widely used by the LHC collaborations: PYTHIA8 with the standard Monash tune, which includes colour re-connection as final-state effects [13], PYTHIA8 Monash tune with shoving [14] and EPOS LHC [12]. It is important to note that the PYTHIA 8 Monash and EPOS LHC tunings were based on single-particle spectra and underlying event observables, but did not include particle correlations in azimuth. The shoving strenght parameter g is here set to $g=3$ and in

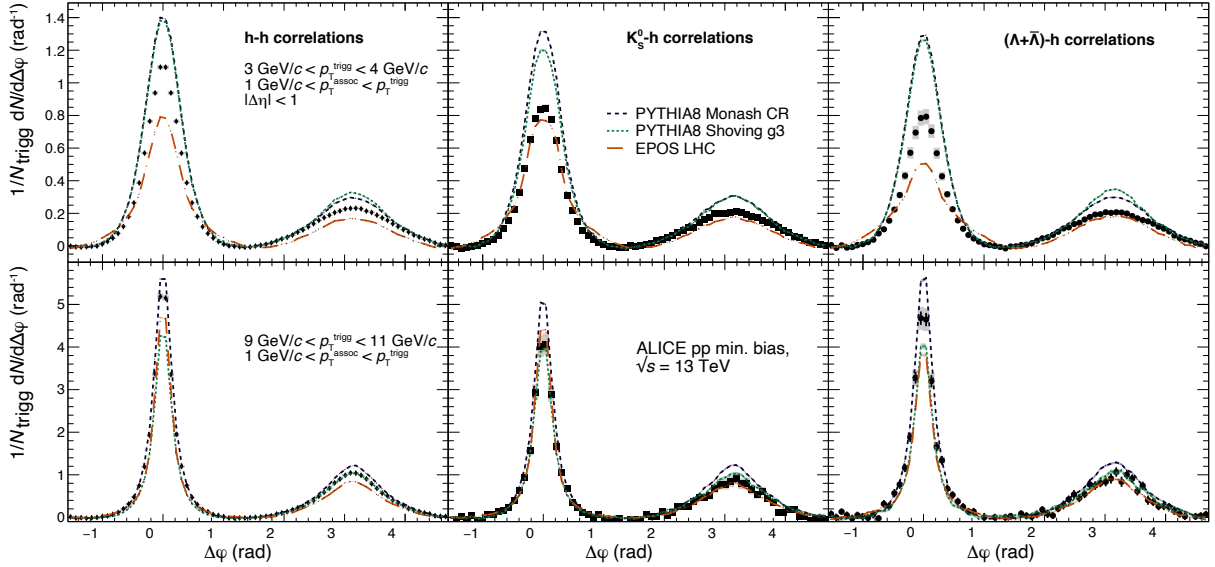


Figure 2: $\Delta\phi$ projection of the h-h (left), K_S^0 -h (middle) and $(\Lambda + \bar{\Lambda})$ -h (right) correlation functions compared with MC event generators for low (top) and high (bottom) p_T^{trigg} . Error bars and colored boxes represent statistical and systematic uncertainties, respectively. The data are compared with MC event generators.

addition the upper p_T cut for the shoving mechanism is turned off. None of the models describes quantitatively the correlation functions consistently for the three trigger particle species. For the low p_T^{trigg} , both PYTHIA8 tunes overestimate the peaks on the near- and away-side, while EPOS LHC underestimates them significantly for all trigger particles except for the K_S^0 . In the high p_T^{trigg} interval, the shoving tune of PYTHIA8 is underestimating the near-side peak for all trigger particles except for K_S^0 -h case, but describes well the away-side peak. The description of EPOS LHC and PYTHIA8 Monash is similar in both p_T^{trigg} intervals, where EPOS LHC is underestimating both peaks of h-h and $(\Lambda + \bar{\Lambda})$ -h correlation functions and can reasonably well describe the $\Delta\phi$ projection of the K_S^0 -h correlation function. PYTHIA8 Monash tune overestimates both peaks for all three types of correlation functions.

The per-trigger yields, obtained by integrating the $\Delta\phi$ projections of the correlation function for the intervals $|\Delta\phi| < 0.9$ (near-side) and $|\Delta\phi - \pi| < 1.4$ (away-side) are studied as a function of p_T^{trigg} , p_T^{assoc} and event-activity class for the three trigger particle species and compared with the MC event generators. The results are described in the following sections.

4.1 Per-trigger yields

The per-trigger yields are shown in Fig. 3 as a function of the p_T^{trigg} for different event-activity classes. An increasing trend with p_T^{trigg} is observed, as expected, as higher energetic jets have increasingly more associated particles.

For a more quantitative inspection of the event-activity dependence, the ratio between the yield in each event class and the yield for minimum bias is given in Fig. 4. Different trends are visible for the near- and away-side peaks. A clear multiplicity ordering for the near-side can be observed, events with higher multiplicity exhibiting the highest yields. This behaviour is most obvious for the h-h correlations, but it is significant on the near-side also for the V^0 -triggered yields.

For the away-side this ordering is reverted, in particular with the increase of the p_T of the trigger particle. Given the uncertainties, this trend is less significant for the K_S^0 -h and $(\Lambda + \bar{\Lambda})$ -h correlations. The finding is qualitatively reproduced in PYTHIA8 simulations and can be understood considering that the location of the away-side jet is not fixed in η . The requirement of a low (high) multiplicity in the V0 detectors at larger rapidity, biases the events towards configurations where the away-side jet is within (outside)

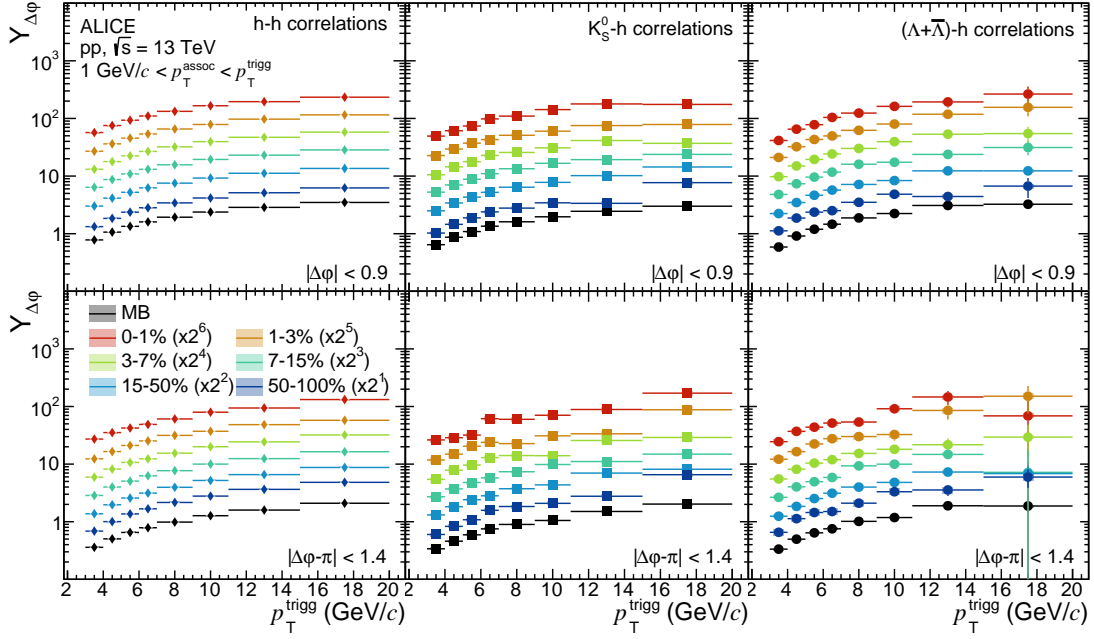


Figure 3: Per-trigger yields of h-h (left), K_S^0 -h (middle) and $(\Lambda + \bar{\Lambda})$ -h (right) correlation functions as a function of p_T^{trigg} on the near-side (upper row) and away-side (lower row) for different multiplicity classes. For visibility, the values in the various event classes are scaled with the factors indicated in the legend. Error bars and colored boxes represent statistical and systematic uncertainties, respectively, which are in most cases within the data points.

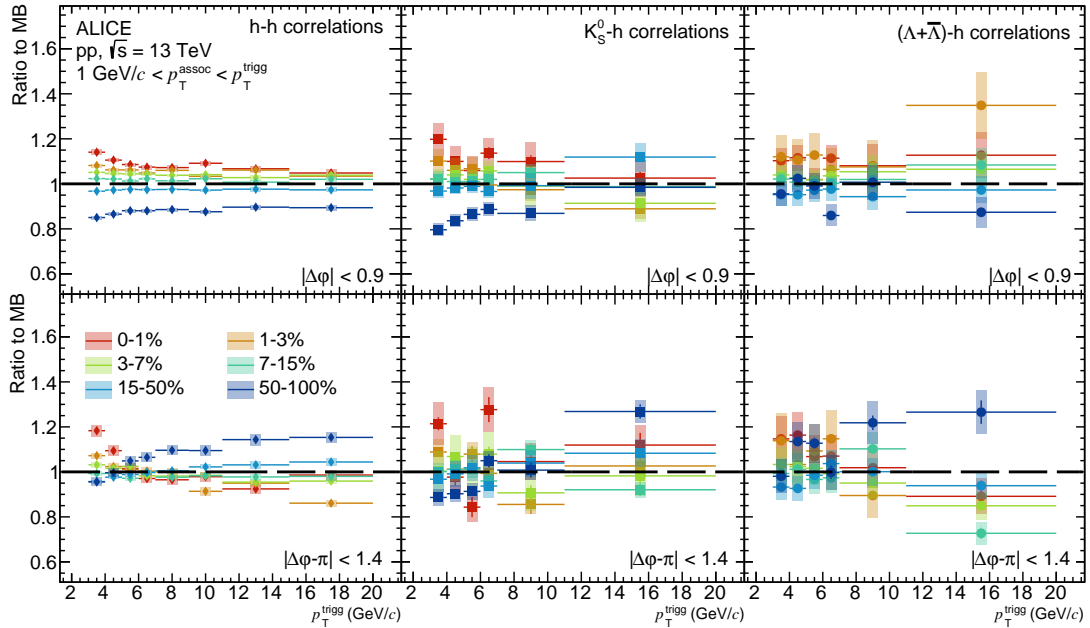


Figure 4: Ratio of the per-trigger yields in different multiplicity classes to the corresponding minimum bias yield for h-h (left), K_S^0 -h (middle) and $(\Lambda + \bar{\Lambda})$ -h (right) correlations on the near-side (upper row) and away-side (lower row). Error bars and colored boxes represent statistical and systematic uncertainties, respectively.

the central acceptance, thus increasing (decreasing) the per-trigger yield at the away-side. The near-side jet is by construction in the central pseudorapidity acceptance, though the multiplicity measurement in the V0 detectors may still be influenced by long range correlations (flow-like) and fragmentation biases. This jet bias, although expected and roughly understood, is interesting, as it gives insights on particle production mechanisms. It is further investigated through the comparison with model predictions and

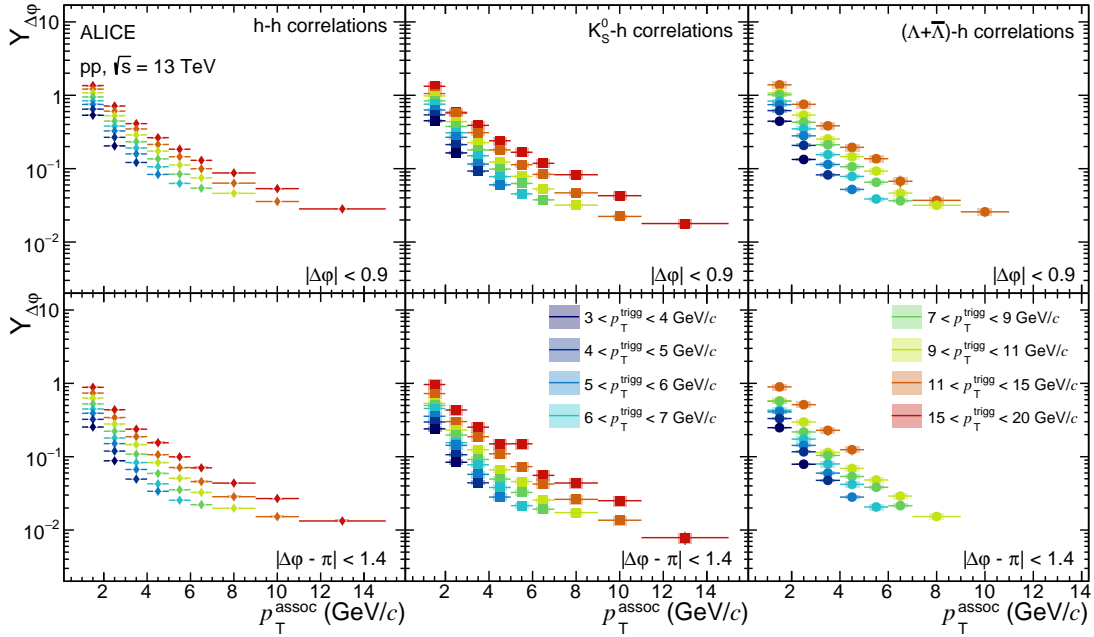


Figure 5: Per-trigger yields of h-h (left), K_S^0 -h (middle) and $(\Lambda + \bar{\Lambda})$ -h (right) correlation functions as a function of p_T^{assoc} on the near-side (upper row) and away-side (lower row) for different p_T^{trigg} intervals. Error bars and colored boxes represent statistical and systematic uncertainties, respectively.

through normalisation of the yields for K_S^0 -h and $(\Lambda + \bar{\Lambda})$ -h to those for h-h.

The p_T^{assoc} per-trigger yield spectra for different p_T^{trigg} intervals are shown in Fig. 5. A decreasing trend with p_T^{assoc} is observed, as expected, as the probability for creation of associated particle with high p_T decreases with p_T . Note, that due to the kinematic requirement $p_T^{\text{assoc}} < p_T^{\text{trigg}}$, the yields triggered with lower p_T particle do not cover the full p_T^{assoc} range.

4.2 Comparison with model predictions

The ratios of model predictions to data for the integrated per-trigger yields are shown in Fig. 6 for the near- and away-side yields as a function of p_T^{trigg} for minimum bias events and event classes selected on their activity. The first finding is that the trends in the model descriptions of the data are largely the same for h-h, K_S^0 -h and $(\Lambda + \bar{\Lambda})$ -h correlations. The event-activity dependence is reproduced by PYTHIA8 calculations, for both the standard tune and with shoving, the latter clearly offering a better description. The dependence is not reproduced by EPOS LHC.

For the near-side, PYTHIA8 with colour re-connection describes well the yields for high p_T trigger particles while it overestimates the yields at low- p_T . This is valid for all multiplicity classes and holds for the three species of trigger particle. This is a consequence of the good description of the hard QCD processes in PYTHIA8, which do not depend on the event multiplicity. The shoving mechanism improves the intermediate sector, at the price of degrading the harder sector. It is apparent that allowing shoving for large p_T , as done for the simulations presented here, is not entirely physical. The medium-hard and softer regime remains a challenge and is a subject of current theoretical attention [34]. For the away-side, the shoving mechanism describes the data better than the standard PYTHIA8. In EPOS LHC the event-activity dependence seen in data is not described well: a stronger event-activity dependence is observed in the model, which underpredicts the data for higher event multiplicities and either overpredicts it (for the near-side) or describes it well (for the away-side) for the lower event-activity classes.

The features of the data-model comparison are dramatically different in Fig. 7, where the model to data per-trigger yield ratio is shown as a function of p_T^{assoc} for minimum bias collisions. Here, the trigger-

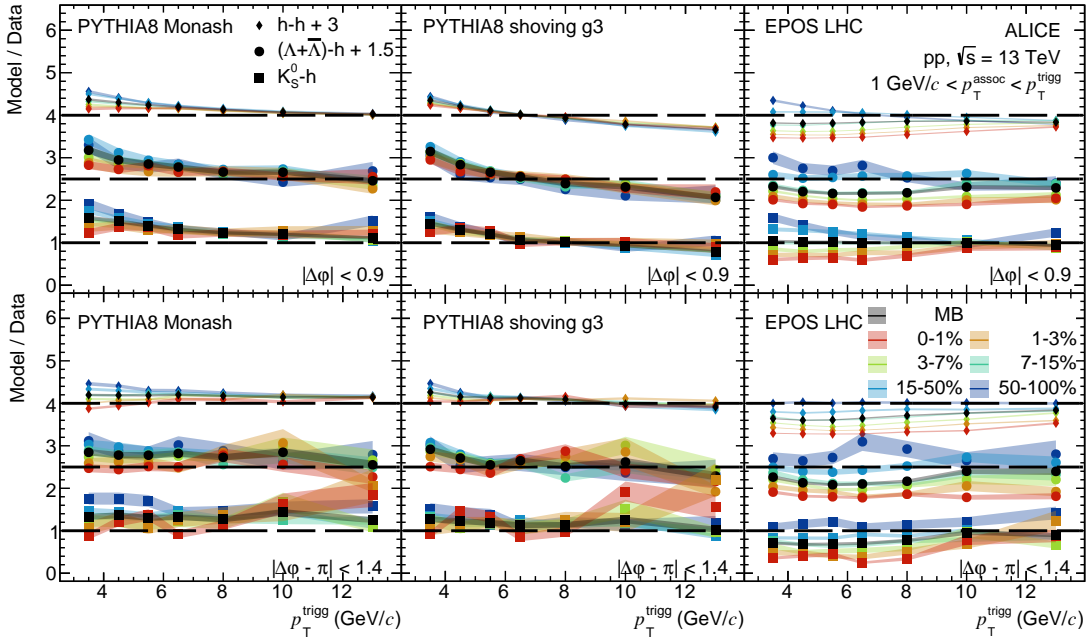


Figure 6: Models to data ratio of integrated per-trigger yields as a function of p_T^{trigg} for different multiplicity classes on the near-side (top panels) and away-side (bottom panels) for three MC event generators: PYTHIA8 Monash with colour re-connection (left), PYTHIA8 with shoving (middle) and EPOS LHC (right). Note, for plotting purpose, the arbitrary shifts for the vertical axis are given in the legend. The bands represent combined systematic and statistical uncertainties from data and models.

particle dependence is rather different in the models. PYTHIA8 predicts, for both the standard settings and for the shoving mechanism, in particular for the near-side and in dependence of p_T^{trigg} , a much stronger dependence on the trigger particle than seen in the data, while EPOS LHC describes the data well. For high values of p_T^{trigg} , the data are described well in the whole p_T^{assoc} range. This reflects that the full fragmentation process in a hard scattering is well modelled. It is important to note that PYTHIA8 Monash describes quite well the measured p_T dependence of the ratio $(\Lambda + \bar{\Lambda})/K_S^0$ in jets with $p_T > 10$ GeV/c. However, the ratio in MB collisions is not described well, in particular for $p_T < 4$ GeV/c [35].

It is interesting to examine the differences between PYTHIA8 with the standard settings and with the shoving mechanism. Clearly, the shoving mechanism describes the medium-hard processes better, corresponding roughly to $3 < p_T^{\text{trigg}} < 5$ GeV/c and $1 < p_T^{\text{assoc}} < 5$ GeV/c, while the harder processes are underestimated. This is visible in particular in Fig. 6 for all trigger-particle species for different event-activity classes, while in case of the p_T^{assoc} dependence shown in Fig. 7 the shoving mechanism leads to a poorer description of the data compared to the standard settings.

The EPOS LHC model gives a rather different description of the data compared to PYTHIA8. In contrast to the rather poor description of the p_T^{trigg} and event-class dependence (Fig. 6) the dependence on p_T^{assoc} (Fig. 7) is rather well described for different p_T^{trigg} intervals and for the three trigger-particle species.

4.3 Comparison of hadron- and strangeness-triggered yields

In order to compare more quantitatively the correlation yields for different trigger-particle species, ratios to the per-trigger yields for h-h are calculated. These ratios are shown as a function of p_T^{trigg} in Fig. 8 for the near- and away-side, while Fig. 9 shows them as a function of p_T^{assoc} . The data indicate that the differences between charged-hadron (a sample dominated by pions) triggered yields and either K_S^0 or $(\Lambda + \bar{\Lambda})$ triggered yields are small and have a weak dependence on the event-activity class. All three

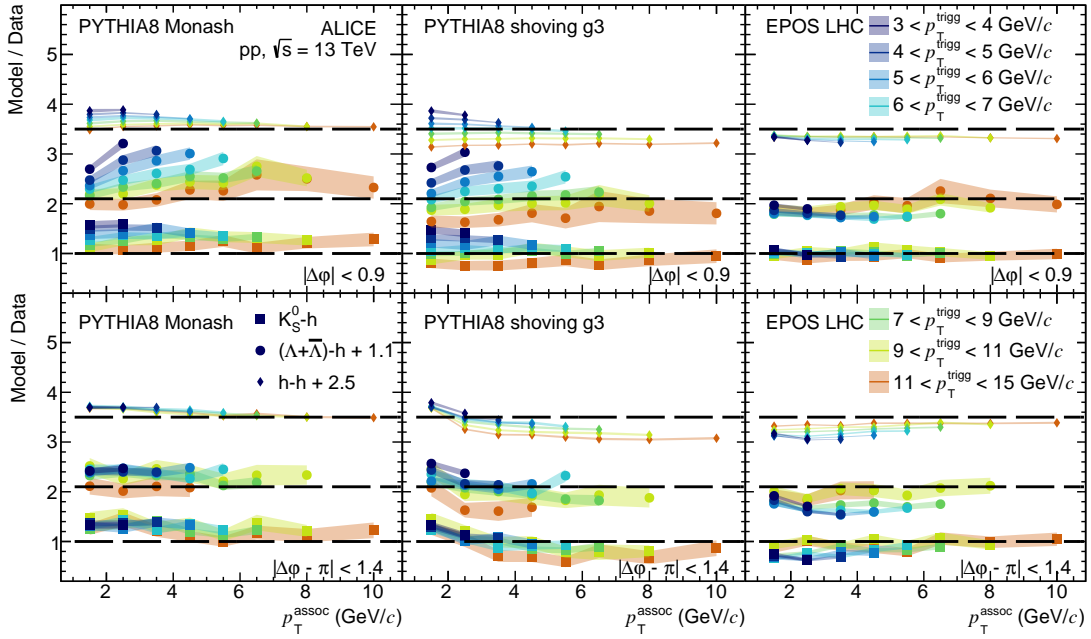


Figure 7: Models to data ratio of integrated per-trigger yields for minimum bias collisions as a function of p_T^{assoc} for different p_T^{trigg} intervals on the near-side (top panels) and away-side (bottom panels) for three MC models: PYTHIA8 Monash with colour re-connection (left), PYTHIA8 with shoving (middle) and EPOS LHC (right). Note that for plotting purpose, the arbitrary shifts for the vertical axis are given in the legend. The bands represent combined systematic and statistical uncertainties for data and statistical for models.

models describe the trends seen in the ratios better than it was the case for yields itself, a consequence of the earlier finding that the model-data disagreements are very similar for the three trigger-particle species.

At closer examination, one observes that a difference between different trigger-particle species is visible for the near-side. The yield ratios $Y_{\Delta\phi}^{K_S^0-h} / Y_{\Delta\phi}^{h-h}$ are smaller than unity and flat with p_T^{trigg} in all multiplicity classes, which indicates that jets triggered with K_S^0 mesons contain less particles than the unbiased (inclusive) jets and this feature does not depend on the hardness of the process (p_T^{trigg}) or event multiplicity. In contrast to that, the $Y_{\Delta\phi}^{(\Lambda+\bar{\Lambda})-h} / Y_{\Delta\phi}^{h-h}$ ratio increases with p_T^{trigg} . Potentially, this could be explained with a bias towards gluon jets, which contain more particles [19] and have relative enhanced production of Λ hyperons [21]. In the right column in the left plot of Fig. 9, it is visible that this effect in the data is pronounced for the soft part of harder jets (low p_T^{assoc} for high p_T^{trigg}). A decreasing trend of the ratio can also be observed with increasing p_T^{assoc} . This suggests that a jet triggered with either a K_S^0 or a Λ or $\bar{\Lambda}$ particle has a smaller amount of associated particles with higher p_T than a jet triggered with an unidentified hadron with the same p_T . This decreasing trend is reproduced by the considered models.

To check if the difference in the ratios for the near side triggered with K_S^0 and $(\Lambda + \bar{\Lambda})$ can be caused by the differences between quark and gluon jets, a separated PYTHIA 8 study was performed, selecting exclusive hard processes containing only quarks ($q + \bar{q} \rightarrow q + \bar{q}$) or gluons ($g + g \rightarrow g + g$) in the final state. The results of this study are shown in Fig. 10 for MB collisions in comparison with the data. It is visible that the ratio is almost identical for the K_S^0 -triggered yields for both quark and gluon jets. In this case, for both processes the ratio is flat as a function of p_T^{trigg} and decreasing with p_T^{assoc} . Nevertheless, a clear difference between the two processes is observed in the ratios of yields triggered with $(\Lambda + \bar{\Lambda})$. The ratio for the gluon-jet process is increasing with p_T^{trigg} and is higher, while it is flat and smaller for the quark jets. A systematic difference is visible also in the p_T^{assoc} dependence, where the ratio from gluon jets is significantly higher than the one from quark jets. Although the p_T distributions of hadrons in

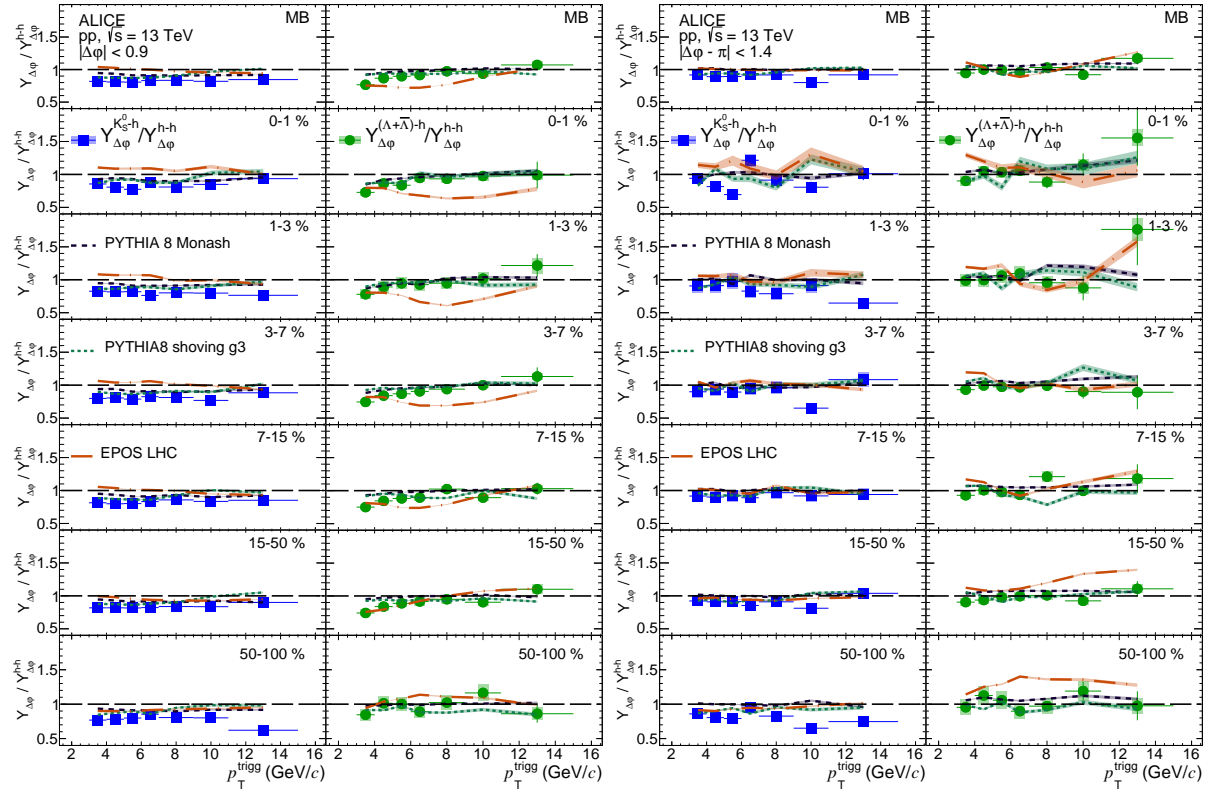


Figure 8: Ratios of integrated per-trigger yield of K_S^0 -h (left column) or $(\Lambda + \bar{\Lambda})$ -h (right column) to h-h as a function of p_T^{trigg} , for the near-side in the left plot and for the away-side in the right plot, for different event multiplicity classes. Error bars and colored boxes represent statistical and systematic uncertainties, respectively. The bands around model curves stand for their statistical uncertainty.

the simulated exclusive processes may be different than in MB collisions, it is expected that the observed difference is generic and explains at least some of the trends seen in the data.

In contrast, for the away-side, the ratios as a function of p_T^{trigg} are compatible with unity within the uncertainties as shown in the right part of Fig. 8, thus no dependence on the trigger particle species (K_S^0 or $(\Lambda + \bar{\Lambda})$) is seen. The deviation of some bins from unity is caused by the fluctuations affecting the underlying event estimation. A similar trend is also observed in the p_T^{assoc} dependence in the right plot of Fig. 9. This fits to the expectation that there is no bias in the away-side jet, since the associated production of strangeness is not dominated by hard processes, i.e. initial production of a $s\bar{s}$ pair leading to two strangeness induced jets. This is confirmed by the comparison with models, which predict ratios for the away-side around unity (Fig. 8).

5 Summary and conclusions

Charged-hadron, K_S^0 and $(\Lambda + \bar{\Lambda})$ triggered correlation functions are measured at the LHC in pp collisions at $\sqrt{s} = 13$ TeV with the ALICE apparatus. The integrated per-trigger yields are extracted for both near- and away-side and studied as a function of event multiplicity, p_T^{trigg} and p_T^{assoc} . A dependence on the event-multiplicity is observed, which may be explained at the near-side by an interplay of fragmentation and of collective-like effects such as the long-range ridge. For the away-side the primary effects are likely due to a selection bias, where the away-side jet is within the V0 detector acceptance causing smaller away-side yields for high-multiplicity classes. This bias was overcome by studying the ratios of yields for K_S^0 or $(\Lambda + \bar{\Lambda})$ as trigger particle over that for inclusive hadrons. For the near-side, different trends were observed for yield ratios triggered by K_S^0 and $(\Lambda + \bar{\Lambda})$. While the $Y_{\Delta\phi}^{K_S^0-h} / Y_{\Delta\phi}^{h-h}$ is flat,

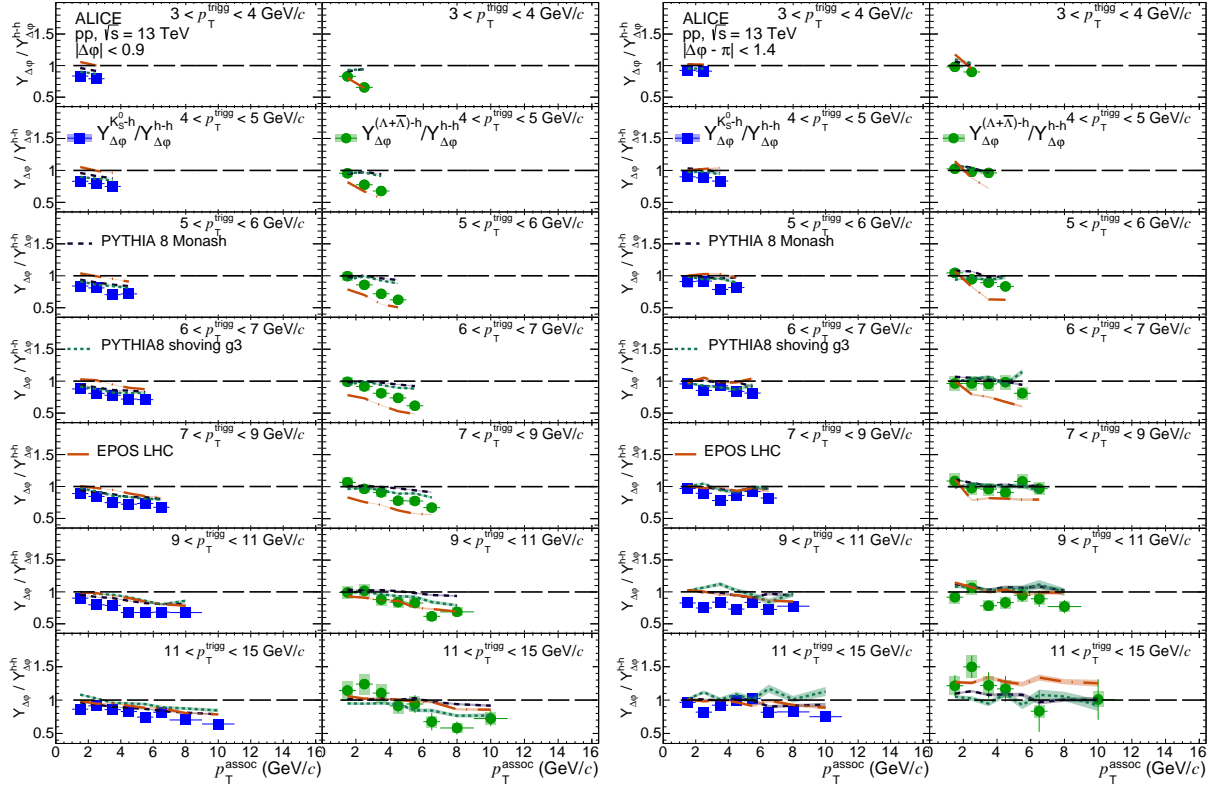


Figure 9: Per-trigger yield ratios of K_S^0 -h (left column) or $(\Lambda + \bar{\Lambda})$ -h (right column) to h-h as a function of p_T^{assoc} , for the near-side in the left plot and for the away-side in the right plot, for different p_T^{trigg} intervals in the MB sample. Error bars and colored boxes represent statistical and systematic uncertainties, respectively. The bands around model curves stand for their statistical uncertainty.

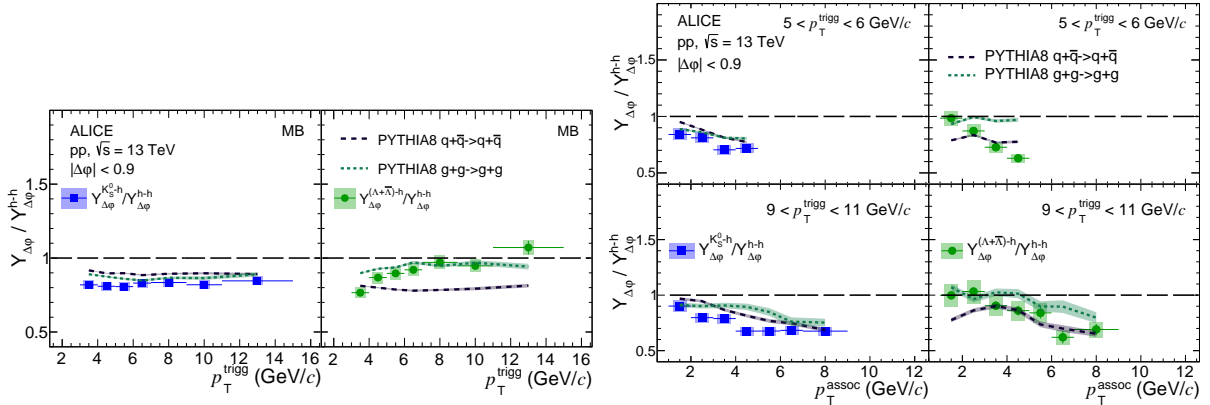


Figure 10: Per-trigger yield ratios of K_S^0 -h (left column) or $(\Lambda + \bar{\Lambda})$ -h (right column) to h-h at the near-side as a function of p_T^{trigg} in the left plot and as a function of p_T^{assoc} in the right plot, compared with the PYTHIA8 calculation of the quark and gluon jets. Error bars and colored boxes represent statistical and systematic uncertainties, respectively. The bands around model curves stand for their statistical uncertainty.

the $Y_{\Delta\phi}^{(\Lambda+\bar{\Lambda})-h}/Y_{\Delta\phi}^{h-h}$ increases with p_T^{trigg} . This difference is most pronounced for high p_T^{trigg} and low p_T^{assoc} . A PYTHIA8 study of the respective exclusive processes reveals that the difference is caused by the bias towards gluon jets through triggering with Λ or $\bar{\Lambda}$ hyperon. In the p_T^{assoc} dependence of these yield ratios, a decreasing trend of the ratio can be observed with increasing p_T^{assoc} , suggesting a smaller amount of associated particles with higher p_T in the jets triggered with a V^0 particle than in jets triggered with an unidentified hadron with the same p_T . This trend can be reproduced by the considered models.

However, on the away-side, no clear difference between the trigger-particle species is observed.

All the measured quantities are compared with model predictions. PYTHIA8 with the standard Monash tune can describe the data for high p_T^{trigg} (hard processes) while the shoving mechanism works better at intermediate p_T^{trigg} . The comparison of data with the EPOS LHC model reveals that the model predicts a significantly stronger multiplicity dependence than seen in the data. The ratios of yields for K_S⁰ or (Λ + $\bar{\Lambda}$) trigger particles to those for inclusive (charged) hadrons are qualitatively well described by all the considered models, except for EPOS LHC at the near-side for the (Λ + $\bar{\Lambda}$) triggered yield ratios.

Acknowledgements

The ALICE Collaboration would like to thank Christian Bierlich for providing the PYTHIA8 String Shoving configurations and discussions around this and Tanguy Pierog and Klaus Werner for helpful discussions around the EPOS LHC model.

The ALICE Collaboration would like to thank all its engineers and technicians for their invaluable contributions to the construction of the experiment and the CERN accelerator teams for the outstanding performance of the LHC complex. The ALICE Collaboration gratefully acknowledges the resources and support provided by all Grid centres and the Worldwide LHC Computing Grid (WLCG) collaboration. The ALICE Collaboration acknowledges the following funding agencies for their support in building and running the ALICE detector: A. I. Alikhanyan National Science Laboratory (Yerevan Physics Institute) Foundation (ANSL), State Committee of Science and World Federation of Scientists (WFS), Armenia; Austrian Academy of Sciences, Austrian Science Fund (FWF): [M 2467-N36] and Nationalstiftung für Forschung, Technologie und Entwicklung, Austria; Ministry of Communications and High Technologies, National Nuclear Research Center, Azerbaijan; Conselho Nacional de Desenvolvimento Científico e Tecnológico (CNPq), Financiadora de Estudos e Projetos (Finep), Fundação de Amparo à Pesquisa do Estado de São Paulo (FAPESP) and Universidade Federal do Rio Grande do Sul (UFRGS), Brazil; Ministry of Education of China (MOEC), Ministry of Science & Technology of China (MSTC) and National Natural Science Foundation of China (NSFC), China; Ministry of Science and Education and Croatian Science Foundation, Croatia; Centro de Aplicaciones Tecnológicas y Desarrollo Nuclear (CEADEN), Cubaenergía, Cuba; Ministry of Education, Youth and Sports of the Czech Republic, Czech Republic; The Danish Council for Independent Research | Natural Sciences, the VILLUM FONDEN and Danish National Research Foundation (DNRF), Denmark; Helsinki Institute of Physics (HIP), Finland; Commissariat à l’Energie Atomique (CEA) and Institut National de Physique Nucléaire et de Physique des Particules (IN2P3) and Centre National de la Recherche Scientifique (CNRS), France; Bundesministerium für Bildung und Forschung (BMBF) and GSI Helmholtzzentrum für Schwerionenforschung GmbH, Germany; General Secretariat for Research and Technology, Ministry of Education, Research and Religions, Greece; National Research, Development and Innovation Office, Hungary; Department of Atomic Energy Government of India (DAE), Department of Science and Technology, Government of India (DST), University Grants Commission, Government of India (UGC) and Council of Scientific and Industrial Research (CSIR), India; Indonesian Institute of Science, Indonesia; Istituto Nazionale di Fisica Nucleare (INFN), Italy; Institute for Innovative Science and Technology, Nagasaki Institute of Applied Science (IIST), Japanese Ministry of Education, Culture, Sports, Science and Technology (MEXT) and Japan Society for the Promotion of Science (JSPS) KAKENHI, Japan; Consejo Nacional de Ciencia (CONACYT) y Tecnología, through Fondo de Cooperación Internacional en Ciencia y Tecnología (FONCICYT) and Dirección General de Asuntos del Personal Académico (DGAPA), Mexico; Nederlandse Organisatie voor Wetenschappelijk Onderzoek (NWO), Netherlands; The Research Council of Norway, Norway; Commission on Science and Technology for Sustainable Development in the South (COMSATS), Pakistan; Pontificia Universidad Católica del Perú, Peru; Ministry of Education and Science, National Science Centre and WUT ID-UB, Poland; Korea Institute of Science and Technology Information and National Research Foundation of Korea (NRF), Republic of Korea; Ministry of

Education and Scientific Research, Institute of Atomic Physics and Ministry of Research and Innovation and Institute of Atomic Physics, Romania; Joint Institute for Nuclear Research (JINR), Ministry of Education and Science of the Russian Federation, National Research Centre Kurchatov Institute, Russian Science Foundation and Russian Foundation for Basic Research, Russia; Ministry of Education, Science, Research and Sport of the Slovak Republic, Slovakia; National Research Foundation of South Africa, South Africa; Swedish Research Council (VR) and Knut & Alice Wallenberg Foundation (KAW), Sweden; European Organization for Nuclear Research, Switzerland; Suranaree University of Technology (SUT), National Science and Technology Development Agency (NSDTA) and Office of the Higher Education Commission under NRU project of Thailand, Thailand; Turkish Energy, Nuclear and Mineral Research Agency (TENMAK), Turkey; National Academy of Sciences of Ukraine, Ukraine; Science and Technology Facilities Council (STFC), United Kingdom; National Science Foundation of the United States of America (NSF) and United States Department of Energy, Office of Nuclear Physics (DOE NP), United States of America.

References

- [1] CMS Collaboration, V. Khachatryan *et al.*, “Observation of Long-Range Near-Side Angular Correlations in Proton-Proton Collisions at the LHC”, *JHEP* **09** (2010) 091, arXiv:1009.4122 [hep-ex].
- [2] CMS Collaboration, V. Khachatryan *et al.*, “Measurement of long-range near-side two-particle angular correlations in pp collisions at $\sqrt{s} = 13$ TeV”, *Phys. Rev. Lett.* **116** no. 17, (2016) 172302, arXiv:1510.03068 [nucl-ex].
- [3] ATLAS Collaboration, G. Aad *et al.*, “Observation of Long-Range Elliptic Azimuthal Anisotropies in $\sqrt{s} = 13$ and 2.76 TeV *pp* Collisions with the ATLAS Detector”, *Phys. Rev. Lett.* **116** no. 17, (2016) 172301, arXiv:1509.04776 [hep-ex].
- [4] CMS Collaboration, V. Khachatryan *et al.*, “Evidence for collectivity in pp collisions at the LHC”, *Phys. Lett. B* **765** (2017) 193–220, arXiv:1606.06198 [nucl-ex].
- [5] ALICE Collaboration, J. Adam *et al.*, “Enhanced production of multi-strange hadrons in high-multiplicity proton-proton collisions”, *Nature Phys.* **13** (2017) 535–539, arXiv:1606.07424 [nucl-ex].
- [6] ALICE Collaboration, S. Acharya *et al.*, “Multiplicity dependence of (multi-)strange hadron production in proton-proton collisions at $\sqrt{s} = 13$ TeV”, *Eur. Phys. J.* **C80** no. 2, (2020) 167, arXiv:1908.01861 [nucl-ex].
- [7] K. Dusling and R. Venugopalan, “Evidence for BFKL and saturation dynamics from dihadron spectra at the LHC”, *Phys. Rev. D* **87** no. 5, (2013) 051502, arXiv:1210.3890 [hep-ph].
- [8] B. Schenke, C. Shen, and P. Tribedy, “Running the gamut of high energy nuclear collisions”, *Phys. Rev. C* **102** no. 4, (2020) 044905, arXiv:2005.14682 [nucl-th].
- [9] K. Dusling, W. Li, and B. Schenke, “Novel collective phenomena in high-energy proton–proton and proton–nucleus collisions”, *Int. J. Mod. Phys. E* **25** no. 01, (2016) 1630002, arXiv:1509.07939 [nucl-ex].
- [10] B. Schenke, “The smallest fluid on earth”, arXiv:2102.11189 [nucl-th].
- [11] T. Sjöstrand, S. Ask, J. R. Christiansen, R. Corke, N. Desai, P. Ilten, S. Mrenna, S. Prestel, C. O. Rasmussen, and P. Z. Skands, “An Introduction to PYTHIA 8.2”, *Comput. Phys. Commun.* **191** (2015) 159–177, arXiv:1410.3012 [hep-ph].
- [12] T. Pierog, I. Karpenko, J. M. Katzy, E. Yatsenko, and K. Werner, “EPOS LHC: Test of collective hadronization with data measured at the CERN Large Hadron Collider”, *Phys. Rev. C* **92** no. 3, (2015) 034906, arXiv:1306.0121 [hep-ph].
- [13] P. Skands, S. Carrazza, and J. Rojo, “Tuning PYTHIA 8.1: the Monash 2013 Tune”, *Eur. Phys. J.* **C74** no. 8, (2014) 3024, arXiv:1404.5630 [hep-ph].
- [14] C. Bierlich, G. Gustafson, and L. Lönnblad, “Collectivity without plasma in hadronic collisions”, *Phys. Lett. B* **779** (2018) 58–63, arXiv:1710.09725 [hep-ph].
- [15] C. Bierlich, “Soft modifications to jet fragmentation in high energy proton–proton collisions”, *Phys. Lett. B* **795** (2019) 194–199, arXiv:1901.07447 [hep-ph].

- [16] J. Adam, D. Adamová, M. Aggarwal, G. Aglieri Rinella, M. Agnello, N. Agrawal, Z. Ahammed, S. Ahn, I. Aimo, S. Aiola, and et al., “Measurement of charged jet production cross sections and nuclear modification in p–pb collisions at $\sqrt{s}=5.02$ tev”, *Physics Letters B* **749** (Oct, 2015) 68–81. <http://dx.doi.org/10.1016/j.physletb.2015.07.054>.
- [17] **ATLAS** Collaboration, M. Aaboud *et al.*, “Measurement of long-range two-particle azimuthal correlations in Z-boson tagged pp collisions at $\sqrt{s}=8$ and 13 TeV”, *Eur. Phys. J. C* **80** no. 1, (2020) 64, arXiv:1906.08290 [nucl-ex].
- [18] **ALICE** Collaboration, S. Acharya *et al.*, “Long- and short-range correlations and their event-scale dependence in high-multiplicity pp collisions at $\sqrt{s} = 13$ TeV”, *JHEP* **05** (2021) 290, arXiv:2101.03110 [nucl-ex].
- [19] **OPAL** Collaboration, G. Abbiendi *et al.*, “Particle multiplicity of unbiased gluon jets from e+e-three-jet events”, *Eur. Phys. J. C* **23** (2002) 597–613, arXiv:hep-ex/0111013.
- [20] **DELPHI** Collaboration, “Energy dependence of the differences between the quark and gluon jet fragmentation”, *Z Phys C - Particles and Fields* **70** (1996) . <https://doi.org/10.1007/s002880050095>.
- [21] **OPAL** Collaboration, K. Ackerstaff *et al.*, “Production of K_S^0 and Λ in quark and gluon jets from Z^0 decay”, *Eur. Phys. J. C* **8** (1999) 241–254, arXiv:9805025 [hep-ex].
- [22] **ALICE** Collaboration, B. Abelev *et al.*, “The ALICE experiment at the CERN LHC”, *JINST* **3** (2008) S08002. <https://doi.org/10.1088/1748-0221/3/08/s08002>.
- [23] **ALICE** Collaboration, B. Abelev *et al.*, “Performance of the ALICE Experiment at the CERN LHC”, *Int. J. Mod. Phys. A* **29** (2014) 1430044, arXiv:1402.4476 [nucl-ex].
- [24] **ALICE** Collaboration, S. Acharya *et al.*, “Pseudorapidity distributions of charged particles as a function of mid and forward rapidity multiplicities in pp collisions at $\sqrt{s} = 5.02, 7$ and 13 TeV”, arXiv:2009.09434 [nucl-ex].
- [25] **ALICE** Collaboration, S. Acharya *et al.*, “Transverse momentum spectra and nuclear modification factors of charged particles in pp, p-Pb and Pb-Pb collisions at the LHC”, *JHEP* **11** (2018) 013, arXiv:1802.09145 [nucl-ex].
- [26] **Particle Data Group** Collaboration, M. Tanabashi, K. Hagiwara, K. ands Hikasa, *et al.*, “Review of Particle Physics”, *Physical Review D [online]* **98** (Aug, 2018) 030001. <https://link.aps.org/doi/10.1103/PhysRevD.98.030001>.
- [27] **ALICE** Collaboration, S. Acharya *et al.*, “Production of light-flavor hadrons in pp collisions at $\sqrt{s} = 7$ and $\sqrt{s} = 13$ TeV”, *Eur. Phys. J. C* **81** (2021) 256, arXiv:2005.11120 [nucl-ex].
- [28] **ALICE** Collaboration, K. Aamodt *et al.*, “Strange particle production in proton-proton collisions at $\sqrt{s}=0.9$ TeV with ALICE at the LHC”, *Eur. Phys. J. C* (2011), arXiv:1012.3257 [nucl-ex].
- [29] T. Sjöstrand, S. Mrenna, and P. Z. Skands, “A Brief Introduction to PYTHIA 8.1”, *Comput. Phys. Commun.* **178** (2008) 852–867, arXiv:0710.3820 [hep-ph].
- [30] R. Brun *et al.*, “GEANT Detector Description and Simulation Tool”, *CERN-W-5013* (1994) 1.
- [31] **ALICE** Collaboration, J. Adam *et al.*, “Evolution of the longitudinal and azimuthal structure of the near-side jet peak in Pb-Pb collisions at $\sqrt{s_{NN}} = 2.76$ TeV”, *Phys. Rev. C* **96** no. 3, (2017) 034904, arXiv:1609.06667 [nucl-ex].

- [32] T. A. Trainor, “Zero yield at minimum (zyam) method and v_2 : Underestimating jet yields from dihadron azimuth correlations”, *Phys. Rev. C* **81** (Jan, 2010) 014905, arXiv:0904.1733 [hep-ph].
- [33] R. Barlow, “Systematic errors: Facts and fictions”, arXiv:hep-ex/0207026.
- [34] C. Bierlich, S. Chakraborty, G. Gustafson, and L. Lönnblad, “Setting the string shoving picture in a new frame”, *JHEP* **03** (2021) 270, arXiv:2010.07595 [hep-ph].
- [35] **ALICE** Collaboration, S. Acharya *et al.*, “Production of Λ and K_S^0 in jets in p-Pb collisions at $\sqrt{s_{NN}} = 5$ TeV and pp collisions at $\sqrt{s} = 7$ TeV”, arXiv:2105.04890 [nucl-ex].

A The ALICE Collaboration

S. Acharya¹⁴¹, D. Adamová⁹⁶, A. Adler⁷⁴, G. Aglieri Rinella³⁴, M. Agnello³⁰, N. Agrawal⁵⁴, Z. Ahammed¹⁴¹, S. Ahmad¹⁶, S.U. Ahn⁷⁶, I. Ahuja³⁸, Z. Akbar⁵¹, A. Akindinov⁹³, M. Al-Turany¹⁰⁸, S.N. Alam^{16,40}, D. Aleksandrov⁸⁹, B. Alessandro⁵⁹, H.M. Alfanda⁷, R. Alfaro Molina⁷¹, B. Ali¹⁶, Y. Ali¹⁴, A. Alici²⁵, N. Alizadehvandchali¹²⁵, A. Alkin³⁴, J. Alme²¹, T. Alt⁶⁸, L. Altenkamper²¹, I. Altsybeev¹¹³, M.N. Anaam⁷, C. Andrei⁴⁸, D. Andreou⁹¹, A. Andronic¹⁴⁴, M. Angeletti³⁴, V. Anguelov¹⁰⁵, F. Antinori⁵⁷, P. Antonioli⁵⁴, C. Anuj¹⁶, N. Apadula⁸⁰, L. Aphecetche¹¹⁵, H. Appelshäuser⁶⁸, S. Arcelli²⁵, R. Arnaldi⁵⁹, I.C. Arsene²⁰, M. Arslanok^{146,105}, A. Augustinus³⁴, R. Averbeck¹⁰⁸, S. Aziz⁷⁸, M.D. Azmi¹⁶, A. Badalá⁵⁶, Y.W. Baek⁴¹, X. Bai^{129,108}, R. Bailhache⁶⁸, Y. Bailung⁵⁰, R. Bala¹⁰², A. Balbino³⁰, A. Baldisseri¹³⁸, B. Balis², M. Ball⁴³, D. Banerjee⁴, R. Barbera²⁶, L. Barioglio¹⁰⁶, M. Barlou⁸⁵, G.G. Barnaföldi¹⁴⁵, L.S. Barnby⁹⁵, V. Barret¹³⁵, C. Bartels¹²⁸, K. Barth³⁴, E. Bartsch⁶⁸, F. Baruffaldi²⁷, N. Bastid¹³⁵, S. Basu⁸¹, G. Batigne¹¹⁵, B. Batyunya⁷⁵, D. Bauri⁴⁹, J.L. Bazo Alba¹¹², I.G. Bearden⁹⁰, C. Beattie¹⁴⁶, I. Belikov¹³⁷, A.D.C. Bell Hechavarria¹⁴⁴, F. Bellini²⁵, R. Bellwied¹²⁵, S. Belokurova¹¹³, V. Belyaev⁹⁴, G. Bencedi⁶⁹, S. Beole²⁴, A. Bercuci⁴⁸, Y. Berdnikov⁹⁹, A. Berdnikova¹⁰⁵, L. Bergmann¹⁰⁵, M.G. Besoiu⁶⁷, L. Betev³⁴, P.P. Bhaduri¹⁴¹, A. Bhasin¹⁰², I.R. Bhat¹⁰², M.A. Bhat⁴, B. Bhattacharjee⁴², P. Bhattacharya²², L. Bianchi²⁴, N. Bianchi⁵², J. Bielčík³⁷, J. Bielčíková⁹⁶, J. Biernat¹¹⁸, A. Bilandzic¹⁰⁶, G. Biro¹⁴⁵, S. Biswas⁴, J.T. Blair¹¹⁹, D. Blau⁸⁹, M.B. Blidaru¹⁰⁸, C. Blume⁶⁸, G. Boca^{28,58}, F. Bock⁹⁷, A. Bogdanov⁹⁴, S. Boi²², J. Bok⁶¹, L. Boldizsár¹⁴⁵, A. Bolozdynya⁹⁴, M. Bombara³⁸, P.M. Bond³⁴, G. Bonomi^{140,58}, H. Borel¹³⁸, A. Borissov⁸², H. Bossi¹⁴⁶, E. Botta²⁴, L. Bratrud⁶⁸, P. Braun-Munzinger¹⁰⁸, M. Bregant¹²¹, M. Broz³⁷, G.E. Bruno^{107,33}, M.D. Buckland¹²⁸, D. Budnikov¹⁰⁹, H. Buesching⁶⁸, S. Bufalino³⁰, O. Bugnon¹¹⁵, P. Buhler¹¹⁴, Z. Buthelezi^{72,132}, J.B. Butt¹⁴, S.A. Bysiak¹¹⁸, M. Cai^{27,7}, H. Caines¹⁴⁶, A. Caliva¹⁰⁸, E. Calvo Villar¹¹², J.M.M. Camacho¹²⁰, R.S. Camacho⁴⁵, P. Camerini²³, F.D.M. Canedo¹²¹, F. Carnesecchi^{34,25}, R. Caron¹³⁸, J. Castillo Castellanos¹³⁸, E.A.R. Casula²², F. Catalano³⁰, C. Ceballos Sanchez⁷⁵, P. Chakraborty⁴⁹, S. Chandra¹⁴¹, S. Chapeland³⁴, M. Chartier¹²⁸, S. Chattopadhyay¹⁴¹, S. Chattopadhyay¹¹⁰, A. Chauvin²², T.G. Chavez⁴⁵, T. Cheng⁷, C. Cheshkov¹³⁶, B. Cheynis¹³⁶, V. Chibante Barroso³⁴, D.D. Chinellato¹²², S. Cho⁶¹, P. Chochula³⁴, P. Christakoglou⁹¹, C.H. Christensen⁹⁰, P. Christiansen⁸¹, T. Chujo¹³⁴, C. Cicalo⁵⁵, L. Cifarelli²⁵, F. Cindolo⁵⁴, M.R. Ciupek¹⁰⁸, G. Clai^{II,54}, J. Cleymans^{I,124}, F. Colamaria⁵³, J.S. Colburn¹¹¹, D. Colella^{107,53,33,145}, A. Collu⁸⁰, M. Colocci³⁴, M. Concas^{III,59}, G. Conesa Balbastre⁷⁹, Z. Conesa del Valle⁷⁸, G. Contin²³, J.G. Contreras³⁷, M.L. Coquet¹³⁸, T.M. Cormier⁹⁷, P. Cortese³¹, M.R. Cosentino¹²³, F. Costa³⁴, S. Costanza^{28,58}, P. Crochet¹³⁵, R. Cruz-Torres⁸⁰, E. Cuautle⁶⁹, P. Cui⁷, L. Cunqueiro⁹⁷, A. Dainese⁵⁷, M.C. Danisch¹⁰⁵, A. Danu⁶⁷, I. Das¹¹⁰, P. Das⁸⁷, P. Das⁴, S. Das⁴, S. Dash⁴⁹, S. De⁸⁷, A. De Caro²⁹, G. de Cataldo⁵³, L. De Cilladi²⁴, J. de Cuveland³⁹, A. De Falco²², D. De Gruttola²⁹, N. De Marco⁵⁹, C. De Martin²³, S. De Pasquale²⁹, S. Deb⁵⁰, H.F. Degenhardt¹²¹, K.R. Deja¹⁴², L. Dello Stritto²⁹, S. Delsanto²⁴, W. Deng⁷, P. Dhankher¹⁹, D. Di Bari³³, A. Di Mauro³⁴, R.A. Diaz⁸, T. Dietel¹²⁴, Y. Ding^{136,7}, R. Diviá³⁴, D.U. Dixit¹⁹, Ø. Djuvsland²¹, U. Dmitrieva⁶³, J. Do⁶¹, A. Dobrin⁶⁷, B. Dönigus⁶⁸, O. Dordic²⁰, A.K. Dubey¹⁴¹, A. Dubla^{108,91}, S. Dudi¹⁰¹, M. Dukhishyam⁸⁷, P. Dupieux¹³⁵, N. Dzalaiova¹³, T.M. Eder¹⁴⁴, R.J. Ehlers⁹⁷, V.N. Eikeland²¹, F. Eisenhut⁶⁸, D. Elia⁵³, B. Erasmus¹¹⁵, F. Ercolessi²⁵, F. Erhardt¹⁰⁰, A. Erokhin¹¹³, M.R. Ersdal²¹, B. Espagnon⁷⁸, G. Eulisse³⁴, D. Evans¹¹¹, S. Evdokimov⁹², L. Fabbietti¹⁰⁶, M. Faggin²⁷, J. Faivre⁷⁹, F. Fan⁷, A. Fantoni⁵², M. Fasel⁹⁷, P. Fedichio³⁰, A. Feliciello⁵⁹, G. Feofilov¹¹³, A. Fernández Téllez⁴⁵, A. Ferrero¹³⁸, A. Ferretti²⁴, V.J.G. Feuillard¹⁰⁵, J. Figiel¹¹⁸, S. Filchagin¹⁰⁹, D. Finogeev⁶³, F.M. Fionda^{55,21}, G. Fiorenza^{34,107}, F. Flor¹²⁵, A.N. Flores¹¹⁹, S. Foertsch⁷², P. Foka¹⁰⁸, S. Fokin⁸⁹, E. Fragiaco⁶⁰, E. Frajna¹⁴⁵, U. Fuchs³⁴, N. Funicello²⁹, C. Furget⁷⁹, A. Furs⁶³, J.J. Gaardhøje⁹⁰, M. Gagliardi²⁴, A.M. Gago¹¹², A. Gal¹³⁷, C.D. Galvan¹²⁰, P. Ganoti⁸⁵, C. Garabatos¹⁰⁸, J.R.A. Garcia⁴⁵, E. Garcia-Solis¹⁰, K. Garg¹¹⁵, C. Gargiulo³⁴, A. Garibli⁸⁸, K. Garner¹⁴⁴, P. Gasik¹⁰⁸, E.F. Gauger¹¹⁹, A. Gautam¹²⁷, M.B. Gay Ducati⁷⁰, M. Germain¹¹⁵, P. Ghosh¹⁴¹, S.K. Ghosh⁴, M. Giacalone²⁵, P. Gianotti⁵², P. Giubellino^{108,59}, P. Giubilato²⁷, A.M.C. Glaenger¹³⁸, P. Glässel¹⁰⁵, D.J.Q. Goh⁸³, V. Gonzalez¹⁴³, L.H. González-Trueba⁷¹, S. Gorbunov³⁹, M. Gorgon², L. Görlich¹¹⁸, S. Gotovac³⁵, V. Grabski⁷¹, L.K. Graczykowski¹⁴², L. Greiner⁸⁰, A. Grelli⁶², C. Grigoras³⁴, V. Grigoriev⁹⁴, A. Grigoryan^{I,1}, S. Grigoryan^{75,1}, O.S. Groettvik²¹, F. Grosa^{34,59}, J.F. Grosse-Oetringhaus³⁴, R. Grosso¹⁰⁸, G.G. Guardiano¹²², R. Guernane⁷⁹, M. Guilbaud¹¹⁵, K. Gulbrandsen⁹⁰, T. Gunji¹³³, W. Guo⁷, A. Gupta¹⁰², R.G. Gupta¹⁰², S.P. Guzman⁴⁵, L. Gyulai¹⁴⁵, M.K. Habib¹⁰⁸, C. Hadjidakis⁷⁸, G. Halimoglu⁶⁸, H. Hamagaki⁸³, G. Hamar¹⁴⁵, M. Hamid⁷, R. Hannigan¹¹⁹, M.R. Haque^{142,87}, A. Harlanderova¹⁰⁸, J.W. Harris¹⁴⁶, A. Harton¹⁰, J.A. Hasenbichler³⁴, H. Hassan⁹⁷, D. Hatzifotiadiou⁵⁴, P. Hauer⁴³, L.B. Havener¹⁴⁶, S. Hayashi¹³³, S.T. Heckel¹⁰⁶, E. Hellbär¹⁰⁸, H. Helstrup³⁶, T. Herman³⁷, E.G. Hernandez⁴⁵, G. Herrera Corral⁹, F. Herrmann¹⁴⁴, K.F. Hetland³⁶, H. Hillemanns³⁴, C. Hills¹²⁸, B. Hippolyte¹³⁷, B. Hofman⁶², B. Hohlweger⁹¹, J. Honeremann¹⁴⁴, G.H. Hong¹⁴⁷, D. Horak³⁷, S. Hornung¹⁰⁸, A. Horzyk², R. Hosokawa¹⁵, Y. Hou⁷, P. Hristov³⁴, C. Hughes¹³¹, P. Huhn⁶⁸, T.J. Humanic⁹⁸, H. Hushnud¹¹⁰, A. Hutson¹²⁵, D. Hutter³⁹, J.P. Iddon^{34,128}, R. Ilkaev¹⁰⁹, H. Ilyas¹⁴, M. Inaba¹³⁴,

G.M. Innocenti³⁴, M. Ippolitov⁸⁹, A. Isakov^{37,96}, M.S. Islam¹¹⁰, M. Ivanov¹⁰⁸, V. Ivanov⁹⁹, V. Izucheev⁹², M. Jablonski², B. Jacak⁸⁰, N. Jacazio³⁴, P.M. Jacobs⁸⁰, S. Jadlovská¹¹⁷, J. Jadlovsky¹¹⁷, S. Jaelani⁶², C. Jahnke^{122,121}, M.J. Jakubowska¹⁴², A. Jalotra¹⁰², M.A. Janik¹⁴², T. Janson⁷⁴, M. Jercic¹⁰⁰, O. Jevons¹¹¹, A.A.P. Jimenez⁶⁹, F. Jonas^{97,144}, P.G. Jones¹¹¹, J.M. Jowett^{34,108}, J. Jung⁶⁸, M. Jung⁶⁸, A. Junique³⁴, A. Jusko¹¹¹, J. Kaewjai¹¹⁶, P. Kalinak⁶⁴, A. Kalweit³⁴, V. Kaplin⁹⁴, S. Kar⁷, A. Karasu Uysal⁷⁷, D. Karatovic¹⁰⁰, O. Karavichev⁶³, T. Karavicheva⁶³, P. Karczmarczyk¹⁴², E. Karpechev⁶³, A. Kazantsev⁸⁹, U. Kebschull⁷⁴, R. Keidel⁴⁷, D.L.D. Keijdener⁶², M. Keil³⁴, B. Ketzer⁴³, Z. Khabanova⁹¹, A.M. Khan⁷, S. Khan¹⁶, A. Khanzadeev⁹⁹, Y. Kharlov⁹², A. Khatun¹⁶, A. Khuntia¹¹⁸, B. Kileng³⁶, B. Kim^{17,61}, C. Kim¹⁷, D.J. Kim¹²⁶, E.J. Kim⁷³, J. Kim¹⁴⁷, J.S. Kim⁴¹, J. Kim¹⁰⁵, J. Kim¹⁴⁷, J. Kim⁷³, M. Kim¹⁰⁵, S. Kim¹⁸, T. Kim¹⁴⁷, S. Kirsch⁶⁸, I. Kisel³⁹, S. Kiselev⁹³, A. Kisiel¹⁴², J.P. Kitowski², J.L. Klay⁶, J. Klein³⁴, S. Klein⁸⁰, C. Klein-Bösing¹⁴⁴, M. Kleiner⁶⁸, T. Klemenz¹⁰⁶, A. Kluge³⁴, A.G. Knospe¹²⁵, C. Kobdaj¹¹⁶, M.K. Köhler¹⁰⁵, T. Kollegger¹⁰⁸, A. Kondratyev⁷⁵, N. Kondratyeva⁹⁴, E. Kondratyuk⁹², J. König⁶⁸, S.A. Königstorfer¹⁰⁶, P.J. Konopka^{34,2}, G. Kornakov¹⁴², S.D. Koryciak², L. Koska¹¹⁷, A. Kotliarov⁹⁶, O. Kovalenko⁸⁶, V. Kovalenko¹¹³, M. Kowalski¹¹⁸, I. Králik⁶⁴, A. Kravčáková³⁸, L. Kreis¹⁰⁸, M. Krivda^{111,64}, F. Krizek⁹⁶, K. Krizkova Gajdosova³⁷, M. Kroesen¹⁰⁵, M. Krüger⁶⁸, E. Kryshen⁹⁹, M. Krzewicki³⁹, V. Kučera³⁴, C. Kuhn¹³⁷, P.G. Kuijjer⁹¹, T. Kumaoka¹³⁴, D. Kumar¹⁴¹, L. Kumar¹⁰¹, N. Kumar¹⁰¹, S. Kundu^{34,87}, P. Kurashvili⁸⁶, A. Kurepin⁶³, A.B. Kurepin⁶³, A. Kuryakin¹⁰⁹, S. Kushpil⁹⁶, J. Kvapil¹¹¹, M.J. Kweon⁶¹, J.Y. Kwon⁶¹, Y. Kwon¹⁴⁷, S.L. La Pointe³⁹, P. La Rocca²⁶, Y.S. Lai⁸⁰, A. Lakrathok¹¹⁶, M. Lamanna³⁴, R. Langoy¹³⁰, K. Lapidus³⁴, P. Larionov^{34,52}, E. Laudi³⁴, L. Lautner^{34,106}, R. Lavicka³⁷, T. Lazareva¹¹³, R. Lea^{140,23,58}, J. Lehrbach³⁹, R.C. Lemmon⁹⁵, I. León Monzón¹²⁰, E.D. Lesser¹⁹, M. Lettrich^{34,106}, P. Lévai¹⁴⁵, X. Li¹¹, X.L. Li⁷, J. Lien¹³⁰, R. Lietava¹¹¹, B. Lim¹⁷, S.H. Lim¹⁷, V. Lindenstruth³⁹, A. Lindner⁴⁸, C. Lippmann¹⁰⁸, A. Liu¹⁹, D.H. Liu⁷, J. Liu¹²⁸, I.M. Lofnes²¹, V. Loginov⁹⁴, C. Loizides⁹⁷, P. Loncar³⁵, J.A. Lopez¹⁰⁵, X. Lopez¹³⁵, E. López Torres⁸, J.R. Luhder¹⁴⁴, M. Lunardon²⁷, G. Luparello⁶⁰, Y.G. Ma⁴⁰, A. Maevskaya⁶³, M. Mager³⁴, T. Mahmoud⁴³, A. Maire¹³⁷, M. Malaev⁹⁹, N.M. Malik¹⁰², Q.W. Malik²⁰, L. Malinina^{IV,75}, D. Mal'Kevich⁹³, N. Mallick⁵⁰, P. Malzacher¹⁰⁸, G. Mandaglio^{32,56}, V. Manko⁸⁹, F. Manso¹³⁵, V. Manzari⁵³, Y. Mao⁷, J. Mareš⁶⁶, G.V. Margagliotti²³, A. Margotti⁵⁴, A. Marín¹⁰⁸, C. Markert¹¹⁹, M. Marquard⁶⁸, N.A. Martin¹⁰⁵, P. Martinengo³⁴, J.L. Martinez¹²⁵, M.I. Martínez⁴⁵, G. Martínez García¹¹⁵, S. Masciocchi¹⁰⁸, M. Masera²⁴, A. Masoni⁵⁵, L. Massacrier⁷⁸, A. Mastroserio^{139,53}, A.M. Mathis¹⁰⁶, O. Matonoha⁸¹, P.F.T. Matuoka¹²¹, A. Matyja¹¹⁸, C. Mayer¹¹⁸, A.L. Mazuecos³⁴, F. Mazzaschi²⁴, M. Mazzilli³⁴, J.E. Mdhuli¹³², A.F. Mechler⁶⁸, Y. Melikyan⁶³, A. Menchaca-Rocha⁷¹, E. Meninno^{114,29}, A.S. Menon¹²⁵, M. Meres¹³, S. Mhlanga^{124,72}, Y. Miake¹³⁴, L. Micheletti^{59,24}, L.C. Migliorin¹³⁶, D.L. Mihaylov¹⁰⁶, K. Mikhaylov^{75,93}, A.N. Mishra¹⁴⁵, D. Miśkowiec¹⁰⁸, A. Modak⁴, A.P. Mohanty⁶², B. Mohanty⁸⁷, M. Mohisin Khan^{V,16}, M.A. Molander⁴⁴, Z. Moravcova⁹⁰, C. Mordasini¹⁰⁶, D.A. Moreira De Godoy¹⁴⁴, L.A.P. Moreno⁴⁵, I. Morozov⁶³, A. Morsch³⁴, T. Mrnjavac³⁴, V. Muccifora⁵², E. Mudnic³⁵, D. Mühlheim¹⁴⁴, S. Muhuri¹⁴¹, J.D. Mulligan⁸⁰, A. Mulliri²², M.G. Munhoz¹²¹, R.H. Munzer⁶⁸, H. Murakami¹³³, S. Murray¹²⁴, L. Musa³⁴, J. Musinsky⁶⁴, J.W. Myrcha¹⁴², B. Naik^{132,49}, R. Nair⁸⁶, B.K. Nandi⁴⁹, R. Nania⁵⁴, E. Nappi⁵³, M.U. Naru¹⁴, A.F. Nassirpour⁸¹, A. Nath¹⁰⁵, C. Nattrass¹³¹, A. Neagu²⁰, L. Nellen⁶⁹, S.V. Nesbo³⁶, G. Neskovic³⁹, D. Nesterov¹¹³, B.S. Nielsen⁹⁰, S. Nikolaev⁸⁹, S. Nikulin⁸⁹, V. Nikulin⁹⁹, F. Noferini⁵⁴, S. Noh¹², P. Nomokonov⁷⁵, J. Norman¹²⁸, N. Novitzky¹³⁴, P. Nowakowski¹⁴², A. Nyman⁸⁹, J. Nystrand²¹, M. Ogino⁸³, A. Ohlson⁸¹, V.A. Okorokov⁹⁴, J. Oleniacz¹⁴², A.C. Oliveira Da Silva¹³¹, M.H. Oliver¹⁴⁶, A. Onnerstad¹²⁶, C. Oppedisano⁵⁹, A. Ortiz Velasquez⁶⁹, T. Osako⁴⁶, A. Oskarsson⁸¹, J. Otwinowski¹¹⁸, M. Oya⁴⁶, K. Oyama⁸³, Y. Pachmayer¹⁰⁵, S. Padhan⁴⁹, D. Pagano^{140,58}, G. Paic⁶⁹, A. Palasciano⁵³, J. Pan¹⁴³, S. Panebianco¹³⁸, P. Pareek¹⁴¹, J. Park⁶¹, J.E. Parkkila¹²⁶, S.P. Pathak¹²⁵, R.N. Patra^{102,34}, B. Paul²², H. Pei⁷, T. Peitzmann⁶², X. Peng⁷, L.G. Pereira⁷⁰, H. Pereira Da Costa¹³⁸, D. Peresunko⁸⁹, G.M. Perez⁸, S. Perrin¹³⁸, Y. Pestov⁵, V. Petráček³⁷, M. Petrovici⁴⁸, R.P. Pezzi^{115,70}, S. Piano⁶⁰, M. Pikna¹³, P. Pillot¹¹⁵, O. Pinazza^{54,34}, L. Pinsky¹²⁵, C. Pinto²⁶, S. Pisano⁵², M. Płoskoń⁸⁰, M. Planinic¹⁰⁰, F. Pliquett⁶⁸, M.G. Poghosyan⁹⁷, B. Polichtchouk⁹², S. Politano³⁰, N. Poljak¹⁰⁰, A. Pop⁴⁸, S. Porteboeuf-Houssais¹³⁵, J. Porter⁸⁰, V. Pozdniakov⁷⁵, S.K. Prasad⁴, R. Preghenella⁵⁴, F. Prino⁵⁹, C.A. Pruneau¹⁴³, I. Pshenichnov⁶³, M. Puccio³⁴, S. Qiu⁹¹, L. Quaglia²⁴, R.E. Quishpe¹²⁵, S. Ragoni¹¹¹, A. Rakotozafindrabe¹³⁸, L. Ramello³¹, F. Rami¹³⁷, S.A.R. Ramirez⁴⁵, A.G.T. Ramos³³, T.A. Rancien⁷⁹, R. Raniwala¹⁰³, S. Raniwala¹⁰³, S.S. Räsänen⁴⁴, R. Rath⁵⁰, I. Ravasenga⁹¹, K.F. Read^{97,131}, A.R. Redelbach³⁹, K. Redlich^{VI,86}, A. Rehman²¹, P. Reichelt⁶⁸, F. Reidt³⁴, H.A. Reme-ness³⁶, R. Renfordt⁶⁸, Z. Rescakova³⁸, K. Reygers¹⁰⁵, A. Riabov⁹⁹, V. Riabov⁹⁹, T. Richert⁸¹, M. Richter²⁰, W. Riegler³⁴, F. Riggi²⁶, C. Ristea⁶⁷, M. Rodríguez Cahuantzi⁴⁵, K. Røed²⁰, R. Rogalev⁹², E. Rogochaya⁷⁵, T.S. Rogoschinski⁶⁸, D. Rohr³⁴, D. Röhrich²¹, P.F. Rojas⁴⁵, P.S. Rokita¹⁴², F. Ronchetti⁵², A. Rosano^{32,56}, E.D. Rosas⁶⁹, A. Rossi⁵⁷, A. Rotondi^{28,58}, A. Roy⁵⁰, P. Roy¹¹⁰, S. Roy⁴⁹, N. Rubini²⁵, O.V. Rueda⁸¹, R. Rui²³, B. Ruyantsev⁷⁵, P.G. Russek², A. Rustamov⁸⁸, E. Ryabinkin⁸⁹, Y. Ryabov⁹⁹, A. Rybicki¹¹⁸, H. Rytönen¹²⁶, W. Rzesza¹⁴²,

O.A.M. Saarimaki⁴⁴, R. Sadek¹¹⁵, S. Sadovsky⁹², J. Saetre²¹, K. Šafařík³⁷, S.K. Saha¹⁴¹, S. Saha⁸⁷, B. Sahoo⁴⁹, P. Sahoo⁴⁹, R. Sahoo⁵⁰, S. Sahoo⁶⁵, D. Sahu⁵⁰, P.K. Sahu⁶⁵, J. Saini¹⁴¹, S. Sakai¹³⁴, S. Sambyal¹⁰², V. Samsonov^{1,99,94}, D. Sarkar¹⁴³, N. Sarkar¹⁴¹, P. Sarma⁴², V.M. Sarti¹⁰⁶, M.H.P. Sas¹⁴⁶, J. Schambach^{97,119}, H.S. Scheid⁶⁸, C. Schiaua⁴⁸, R. Schicker¹⁰⁵, A. Schmah¹⁰⁵, C. Schmidt¹⁰⁸, H.R. Schmidt¹⁰⁴, M.O. Schmidt³⁴, M. Schmidt¹⁰⁴, N.V. Schmidt^{97,68}, A.R. Schmier¹³¹, R. Schotter¹³⁷, J. Schukraft³⁴, Y. Schutz¹³⁷, K. Schwarz¹⁰⁸, K. Schweda¹⁰⁸, G. Scioli²⁵, E. Scomparin⁵⁹, J.E. Seger¹⁵, Y. Sekiguchi¹³³, D. Sekihata¹³³, I. Selyuzhenkov^{108,94}, S. Senyukov¹³⁷, J.J. Seo⁶¹, D. Serebryakov⁶³, L. Šerkšnyte¹⁰⁶, A. Sevcenco⁶⁷, T.J. Shaba⁷², A. Shabanov⁶³, A. Shabetai¹¹⁵, R. Shahoyan³⁴, W. Shaikh¹¹⁰, A. Shangaraev⁹², A. Sharma¹⁰¹, H. Sharma¹¹⁸, M. Sharma¹⁰², N. Sharma¹⁰¹, S. Sharma¹⁰², U. Sharma¹⁰², O. Sheibani¹²⁵, K. Shigaki⁴⁶, M. Shimomura⁸⁴, S. Shirinkin⁹³, Q. Shou⁴⁰, Y. Sibiriak⁸⁹, S. Siddhanta⁵⁵, T. Siemiarczuk⁸⁶, T.F. Silva¹²¹, D. Silvermyr⁸¹, G. Simonetti³⁴, B. Singh¹⁰⁶, R. Singh⁸⁷, R. Singh¹⁰², R. Singh⁵⁰, V.K. Singh¹⁴¹, V. Singhal¹⁴¹, T. Sinha¹¹⁰, B. Sitar¹³, M. Sitta³¹, T.B. Skaali²⁰, G. Skorodumovs¹⁰⁵, M. Slupecki⁴⁴, N. Smirnov¹⁴⁶, R.J.M. Snellings⁶², C. Soncco¹¹², J. Song¹²⁵, A. Songmoolnak¹¹⁶, F. Soramel²⁷, S. Sorensen¹³¹, I. Sputowska¹¹⁸, J. Stachel¹⁰⁵, I. Stan⁶⁷, P.J. Steffanic¹³¹, S.F. Stiefelmaier¹⁰⁵, D. Stocco¹¹⁵, I. Storehaug²⁰, M.M. Storetvedt³⁶, C.P. Stylianidis⁹¹, A.A.P. Suaide¹²¹, T. Sugitate⁴⁶, C. Suire⁷⁸, M. Sukhanov⁶³, M. Suljic³⁴, R. Sultanov⁹³, M. Šumbera⁹⁶, V. Sumberia¹⁰², S. Sumowidagdo⁵¹, S. Swain⁶⁵, A. Szabo¹³, I. Szarka¹³, U. Tabassam¹⁴, S.F. Taghavi¹⁰⁶, G. Taillepiet¹³⁵, J. Takahashi¹²², G.J. Tambave²¹, S. Tang^{135,7}, Z. Tang¹²⁹, L.A. Tarasovičová¹⁴⁴, M. Tarhini¹¹⁵, M.G. Tarzila⁴⁸, A. Tauro³⁴, G. Tejada Muñoz⁴⁵, A. Telesca³⁴, L. Terlizzi²⁴, C. Terrevoli¹²⁵, G. Tersimonov³, S. Thakur¹⁴¹, D. Thomas¹¹⁹, R. Tieulent¹³⁶, A. Tikhonov⁶³, A.R. Timmins¹²⁵, M. Tkacik¹¹⁷, A. Toia⁶⁸, N. Topilskaya⁶³, M. Toppi⁵², F. Torales-Acosta¹⁹, T. Tork⁷⁸, S.R. Torres³⁷, A. Trifiro^{32,56}, S. Tripathy^{54,69}, T. Tripathy⁴⁹, S. Trogolo^{34,27}, G. Trombetta³³, V. Trubnikov³, W.H. Trzaska¹²⁶, T.P. Trzcinski¹⁴², B.A. Trzeciak³⁷, A. Tumkin¹⁰⁹, R. Turrisi⁵⁷, T.S. Tveter²⁰, K. Ullaland²¹, A. Uras¹³⁶, M. Urioni^{58,140}, G.L. Usai²², M. Vala³⁸, N. Valle^{58,28}, S. Vallero⁵⁹, N. van der Kolk⁶², L.V.R. van Doremalen⁶², M. van Leeuwen⁹¹, P. Vande Vyvre³⁴, D. Varga¹⁴⁵, Z. Varga¹⁴⁵, M. Varga-Kofarago¹⁴⁵, A. Vargas⁴⁵, M. Vasileiou⁸⁵, A. Vasiliev⁸⁹, O. Vázquez Doce^{52,106}, V. Vechernin¹¹³, E. Vercellin²⁴, S. Vergara Limón⁴⁵, L. Vermunt⁶², R. Vértesi¹⁴⁵, M. Verweij⁶², L. Vickovic³⁵, Z. Vilakazi¹³², O. Villalobos Baillie¹¹¹, G. Vino⁵³, A. Vinogradov⁸⁹, T. Virgili²⁹, V. Vislavicius⁹⁰, A. Vodopyanov⁷⁵, B. Volkel³⁴, M.A. Völkl¹⁰⁵, K. Voloshin⁹³, S.A. Voloshin¹⁴³, G. Volpe³³, B. von Haller³⁴, I. Vorobyev¹⁰⁶, D. Voscek¹¹⁷, N. Vozniuk⁶³, J. Vrláková³⁸, B. Wagner²¹, C. Wang⁴⁰, D. Wang⁴⁰, M. Weber¹¹⁴, R.J.G.V. Weelden⁹¹, A. Wegrzynek³⁴, S.C. Wenzel³⁴, J.P. Wessels¹⁴⁴, J. Wiechula⁶⁸, J. Wikne²⁰, G. Wilk⁸⁶, J. Wilkinson¹⁰⁸, G.A. Willems¹⁴⁴, B. Windelband¹⁰⁵, M. Winn¹³⁸, W.E. Witt¹³¹, J.R. Wright¹¹⁹, W. Wu⁴⁰, Y. Wu¹²⁹, R. Xu⁷, A.K. Yadav¹⁴¹, S. Yalcin⁷⁷, Y. Yamaguchi⁴⁶, K. Yamakawa⁴⁶, S. Yang²¹, S. Yano⁴⁶, Z. Yin⁷, H. Yokoyama⁶², I.-K. Yoo¹⁷, J.H. Yoon⁶¹, S. Yuan²¹, A. Yuncu¹⁰⁵, V. Zaccolo²³, A. Zaman¹⁴, C. Zampolli³⁴, H.J.C. Zanoli⁶², N. Zardoshti³⁴, A. Zarochentsev¹¹³, P. Závada⁶⁶, N. Zaviyalov¹⁰⁹, M. Zhalov⁹⁹, B. Zhang⁷, S. Zhang⁴⁰, X. Zhang⁷, Y. Zhang¹²⁹, V. Zhrebchevskii¹¹³, Y. Zhi¹¹, N. Zhigareva⁹³, D. Zhou⁷, Y. Zhou⁹⁰, J. Zhu^{7,108}, Y. Zhu⁷, A. Zichichi²⁵, G. Zinovjev³, N. Zurlo^{140,58}

Affiliation notes

^I Deceased

^{II} Also at: Italian National Agency for New Technologies, Energy and Sustainable Economic Development (ENEA), Bologna, Italy

^{III} Also at: Dipartimento DET del Politecnico di Torino, Turin, Italy

^{IV} Also at: M.V. Lomonosov Moscow State University, D.V. Skobeltsyn Institute of Nuclear, Physics, Moscow, Russia

^V Also at: Department of Applied Physics, Aligarh Muslim University, Aligarh, India

^{VI} Also at: Institute of Theoretical Physics, University of Wrocław, Poland

Collaboration Institutes

¹ A.I. Alikhanyan National Science Laboratory (Yerevan Physics Institute) Foundation, Yerevan, Armenia

² AGH University of Science and Technology, Cracow, Poland

³ Bogolyubov Institute for Theoretical Physics, National Academy of Sciences of Ukraine, Kiev, Ukraine

⁴ Bose Institute, Department of Physics and Centre for Astroparticle Physics and Space Science (CAPSS), Kolkata, India

⁵ Budker Institute for Nuclear Physics, Novosibirsk, Russia

⁶ California Polytechnic State University, San Luis Obispo, California, United States

- ⁷ Central China Normal University, Wuhan, China
- ⁸ Centro de Aplicaciones Tecnológicas y Desarrollo Nuclear (CEADEN), Havana, Cuba
- ⁹ Centro de Investigación y de Estudios Avanzados (CINVESTAV), Mexico City and Mérida, Mexico
- ¹⁰ Chicago State University, Chicago, Illinois, United States
- ¹¹ China Institute of Atomic Energy, Beijing, China
- ¹² Chungbuk National University, Cheongju, Republic of Korea
- ¹³ Comenius University Bratislava, Faculty of Mathematics, Physics and Informatics, Bratislava, Slovakia
- ¹⁴ COMSATS University Islamabad, Islamabad, Pakistan
- ¹⁵ Creighton University, Omaha, Nebraska, United States
- ¹⁶ Department of Physics, Aligarh Muslim University, Aligarh, India
- ¹⁷ Department of Physics, Pusan National University, Pusan, Republic of Korea
- ¹⁸ Department of Physics, Sejong University, Seoul, Republic of Korea
- ¹⁹ Department of Physics, University of California, Berkeley, California, United States
- ²⁰ Department of Physics, University of Oslo, Oslo, Norway
- ²¹ Department of Physics and Technology, University of Bergen, Bergen, Norway
- ²² Dipartimento di Fisica dell'Università and Sezione INFN, Cagliari, Italy
- ²³ Dipartimento di Fisica dell'Università and Sezione INFN, Trieste, Italy
- ²⁴ Dipartimento di Fisica dell'Università and Sezione INFN, Turin, Italy
- ²⁵ Dipartimento di Fisica e Astronomia dell'Università and Sezione INFN, Bologna, Italy
- ²⁶ Dipartimento di Fisica e Astronomia dell'Università and Sezione INFN, Catania, Italy
- ²⁷ Dipartimento di Fisica e Astronomia dell'Università and Sezione INFN, Padova, Italy
- ²⁸ Dipartimento di Fisica e Nucleare e Teorica, Università di Pavia, Pavia, Italy
- ²⁹ Dipartimento di Fisica 'E.R. Caianiello' dell'Università and Gruppo Collegato INFN, Salerno, Italy
- ³⁰ Dipartimento DISAT del Politecnico and Sezione INFN, Turin, Italy
- ³¹ Dipartimento di Scienze e Innovazione Tecnologica dell'Università del Piemonte Orientale and INFN Sezione di Torino, Alessandria, Italy
- ³² Dipartimento di Scienze MIFT, Università di Messina, Messina, Italy
- ³³ Dipartimento Interateneo di Fisica 'M. Merlin' and Sezione INFN, Bari, Italy
- ³⁴ European Organization for Nuclear Research (CERN), Geneva, Switzerland
- ³⁵ Faculty of Electrical Engineering, Mechanical Engineering and Naval Architecture, University of Split, Split, Croatia
- ³⁶ Faculty of Engineering and Science, Western Norway University of Applied Sciences, Bergen, Norway
- ³⁷ Faculty of Nuclear Sciences and Physical Engineering, Czech Technical University in Prague, Prague, Czech Republic
- ³⁸ Faculty of Science, P.J. Šafárik University, Košice, Slovakia
- ³⁹ Frankfurt Institute for Advanced Studies, Johann Wolfgang Goethe-Universität Frankfurt, Frankfurt, Germany
- ⁴⁰ Fudan University, Shanghai, China
- ⁴¹ Gangneung-Wonju National University, Gangneung, Republic of Korea
- ⁴² Gauhati University, Department of Physics, Guwahati, India
- ⁴³ Helmholtz-Institut für Strahlen- und Kernphysik, Rheinische Friedrich-Wilhelms-Universität Bonn, Bonn, Germany
- ⁴⁴ Helsinki Institute of Physics (HIP), Helsinki, Finland
- ⁴⁵ High Energy Physics Group, Universidad Autónoma de Puebla, Puebla, Mexico
- ⁴⁶ Hiroshima University, Hiroshima, Japan
- ⁴⁷ Hochschule Worms, Zentrum für Technologietransfer und Telekommunikation (ZTT), Worms, Germany
- ⁴⁸ Horia Hulubei National Institute of Physics and Nuclear Engineering, Bucharest, Romania
- ⁴⁹ Indian Institute of Technology Bombay (IIT), Mumbai, India
- ⁵⁰ Indian Institute of Technology Indore, Indore, India
- ⁵¹ Indonesian Institute of Sciences, Jakarta, Indonesia
- ⁵² INFN, Laboratori Nazionali di Frascati, Frascati, Italy
- ⁵³ INFN, Sezione di Bari, Bari, Italy
- ⁵⁴ INFN, Sezione di Bologna, Bologna, Italy
- ⁵⁵ INFN, Sezione di Cagliari, Cagliari, Italy
- ⁵⁶ INFN, Sezione di Catania, Catania, Italy
- ⁵⁷ INFN, Sezione di Padova, Padova, Italy
- ⁵⁸ INFN, Sezione di Pavia, Pavia, Italy

- ⁵⁹ INFN, Sezione di Torino, Turin, Italy
⁶⁰ INFN, Sezione di Trieste, Trieste, Italy
⁶¹ Inha University, Incheon, Republic of Korea
⁶² Institute for Gravitational and Subatomic Physics (GRASP), Utrecht University/Nikhef, Utrecht, Netherlands
⁶³ Institute for Nuclear Research, Academy of Sciences, Moscow, Russia
⁶⁴ Institute of Experimental Physics, Slovak Academy of Sciences, Košice, Slovakia
⁶⁵ Institute of Physics, Homi Bhabha National Institute, Bhubaneswar, India
⁶⁶ Institute of Physics of the Czech Academy of Sciences, Prague, Czech Republic
⁶⁷ Institute of Space Science (ISS), Bucharest, Romania
⁶⁸ Institut für Kernphysik, Johann Wolfgang Goethe-Universität Frankfurt, Frankfurt, Germany
⁶⁹ Instituto de Ciencias Nucleares, Universidad Nacional Autónoma de México, Mexico City, Mexico
⁷⁰ Instituto de Física, Universidade Federal do Rio Grande do Sul (UFRGS), Porto Alegre, Brazil
⁷¹ Instituto de Física, Universidad Nacional Autónoma de México, Mexico City, Mexico
⁷² iThemba LABS, National Research Foundation, Somerset West, South Africa
⁷³ Jeonbuk National University, Jeonju, Republic of Korea
⁷⁴ Johann-Wolfgang-Goethe Universität Frankfurt Institut für Informatik, Fachbereich Informatik und Mathematik, Frankfurt, Germany
⁷⁵ Joint Institute for Nuclear Research (JINR), Dubna, Russia
⁷⁶ Korea Institute of Science and Technology Information, Daejeon, Republic of Korea
⁷⁷ KTO Karatay University, Konya, Turkey
⁷⁸ Laboratoire de Physique des 2 Infinis, Irène Joliot-Curie, Orsay, France
⁷⁹ Laboratoire de Physique Subatomique et de Cosmologie, Université Grenoble-Alpes, CNRS-IN2P3, Grenoble, France
⁸⁰ Lawrence Berkeley National Laboratory, Berkeley, California, United States
⁸¹ Lund University Department of Physics, Division of Particle Physics, Lund, Sweden
⁸² Moscow Institute for Physics and Technology, Moscow, Russia
⁸³ Nagasaki Institute of Applied Science, Nagasaki, Japan
⁸⁴ Nara Women's University (NWU), Nara, Japan
⁸⁵ National and Kapodistrian University of Athens, School of Science, Department of Physics, Athens, Greece
⁸⁶ National Centre for Nuclear Research, Warsaw, Poland
⁸⁷ National Institute of Science Education and Research, Homi Bhabha National Institute, Jatni, India
⁸⁸ National Nuclear Research Center, Baku, Azerbaijan
⁸⁹ National Research Centre Kurchatov Institute, Moscow, Russia
⁹⁰ Niels Bohr Institute, University of Copenhagen, Copenhagen, Denmark
⁹¹ Nikhef, National institute for subatomic physics, Amsterdam, Netherlands
⁹² NRC Kurchatov Institute IHEP, Protvino, Russia
⁹³ NRC «Kurchatov» Institute - ITEP, Moscow, Russia
⁹⁴ NRNU Moscow Engineering Physics Institute, Moscow, Russia
⁹⁵ Nuclear Physics Group, STFC Daresbury Laboratory, Daresbury, United Kingdom
⁹⁶ Nuclear Physics Institute of the Czech Academy of Sciences, Řež u Prahy, Czech Republic
⁹⁷ Oak Ridge National Laboratory, Oak Ridge, Tennessee, United States
⁹⁸ Ohio State University, Columbus, Ohio, United States
⁹⁹ Petersburg Nuclear Physics Institute, Gatchina, Russia
¹⁰⁰ Physics department, Faculty of science, University of Zagreb, Zagreb, Croatia
¹⁰¹ Physics Department, Panjab University, Chandigarh, India
¹⁰² Physics Department, University of Jammu, Jammu, India
¹⁰³ Physics Department, University of Rajasthan, Jaipur, India
¹⁰⁴ Physikalisches Institut, Eberhard-Karls-Universität Tübingen, Tübingen, Germany
¹⁰⁵ Physikalisches Institut, Ruprecht-Karls-Universität Heidelberg, Heidelberg, Germany
¹⁰⁶ Physik Department, Technische Universität München, Munich, Germany
¹⁰⁷ Politecnico di Bari and Sezione INFN, Bari, Italy
¹⁰⁸ Research Division and ExtreMe Matter Institute EMMI, GSI Helmholtzzentrum für Schwerionenforschung GmbH, Darmstadt, Germany
¹⁰⁹ Russian Federal Nuclear Center (VNIIEF), Sarov, Russia
¹¹⁰ Saha Institute of Nuclear Physics, Homi Bhabha National Institute, Kolkata, India
¹¹¹ School of Physics and Astronomy, University of Birmingham, Birmingham, United Kingdom

- 112 Sección Física, Departamento de Ciencias, Pontificia Universidad Católica del Perú, Lima, Peru
- 113 St. Petersburg State University, St. Petersburg, Russia
- 114 Stefan Meyer Institut für Subatomare Physik (SMI), Vienna, Austria
- 115 SUBATECH, IMT Atlantique, Université de Nantes, CNRS-IN2P3, Nantes, France
- 116 Suranaree University of Technology, Nakhon Ratchasima, Thailand
- 117 Technical University of Košice, Košice, Slovakia
- 118 The Henryk Niewodniczanski Institute of Nuclear Physics, Polish Academy of Sciences, Cracow, Poland
- 119 The University of Texas at Austin, Austin, Texas, United States
- 120 Universidad Autónoma de Sinaloa, Culiacán, Mexico
- 121 Universidade de São Paulo (USP), São Paulo, Brazil
- 122 Universidade Estadual de Campinas (UNICAMP), Campinas, Brazil
- 123 Universidade Federal do ABC, Santo Andre, Brazil
- 124 University of Cape Town, Cape Town, South Africa
- 125 University of Houston, Houston, Texas, United States
- 126 University of Jyväskylä, Jyväskylä, Finland
- 127 University of Kansas, Lawrence, Kansas, United States
- 128 University of Liverpool, Liverpool, United Kingdom
- 129 University of Science and Technology of China, Hefei, China
- 130 University of South-Eastern Norway, Tonsberg, Norway
- 131 University of Tennessee, Knoxville, Tennessee, United States
- 132 University of the Witwatersrand, Johannesburg, South Africa
- 133 University of Tokyo, Tokyo, Japan
- 134 University of Tsukuba, Tsukuba, Japan
- 135 Université Clermont Auvergne, CNRS/IN2P3, LPC, Clermont-Ferrand, France
- 136 Université de Lyon, CNRS/IN2P3, Institut de Physique des 2 Infinis de Lyon, Lyon, France
- 137 Université de Strasbourg, CNRS, IPHC UMR 7178, F-67000 Strasbourg, France, Strasbourg, France
- 138 Université Paris-Saclay Centre d'Etudes de Saclay (CEA), IRFU, Département de Physique Nucléaire (DPhN), Saclay, France
- 139 Università degli Studi di Foggia, Foggia, Italy
- 140 Università di Brescia, Brescia, Italy
- 141 Variable Energy Cyclotron Centre, Homi Bhabha National Institute, Kolkata, India
- 142 Warsaw University of Technology, Warsaw, Poland
- 143 Wayne State University, Detroit, Michigan, United States
- 144 Westfälische Wilhelms-Universität Münster, Institut für Kernphysik, Münster, Germany
- 145 Wigner Research Centre for Physics, Budapest, Hungary
- 146 Yale University, New Haven, Connecticut, United States
- 147 Yonsei University, Seoul, Republic of Korea